國 立 中 央 大 學

Physics Department

Master thesis

VUV and EUV irradiation of CH_4+NH_3 ice mixtures

- An implication of Tholin on Charon

研究生: Leung Pui Shan

指導教授: Chen Yu Jung

November 2017

國立中央大學圖書館
碩博士論文電子檔授權書

(101 年 9 月最新修正版)

本授權書授權本人撰寫之碩/博士學位論文全文電子檔(不包含紙本、詳備註 1 說明)，在「國立中央大學圖書館博碩士論文系統」。(以下請擇一勾選)

(　)同意 (立即開放)

(　)同意 (請於西元 ______年_____月_____日開放)

(　)不同意，原因是：______________________________

在國家圖書館「臺灣博碩士論文知識加值系統」

(　)同意 (立即開放)

(　)同意 (請於西元 ______年_____月_____日開放)

(　)不同意，原因是：______________________________

以非專屬、無償授權國立中央大學、台灣聯合大學系統圖書館與國家圖書館，基於推動「資源共享、互惠合作」之理念，於回饋社會與學術研究之目的，得不限地域、時間與次數，以紙本、微縮、光碟及其它各種方法將上列論文收錄、重製、與利用，並得將數位化之上列論文與論文電子檔以上載網路方式，提供讀者基於個人非營利性質之線上檢索、閱覽、下載或列印。

研究生簽名: ____________________　　　學號：____________________

論文名稱:____

指導教授姓名：________________________________

系所　：_____________________所　☐博士班　☐碩士班

備註：

1. 本授權書之授權範圍僅限電子檔，紙本論文部分依著作權法第 15 條第 3 款之規定，採推定原則即預設同意圖書館得公開上架閱覽，如您有申請專利或投稿等考量，不同意紙本上架陳列，須另行加填聲明書，詳細說明與紙本聲明書請至 http://thesis.lib.ncu.edu.tw/ 下載。
2. 本授權書請填寫並**親筆**簽名後，裝訂於各紙本論文封面後之次頁（全文電子檔內之授權書簽名，可用電腦打字代替）。
3. 請加印一份單張之授權書，填寫並親筆簽名後，於辦理離校時交圖書館（以統一代轉寄給國家圖書館）。
4. 讀者基於個人非營利性質之線上檢索、閱覽、下載或列印上列論文，應遵守著作權法規定。

國立中央大學碩士班研究生

論文指導教授推薦書

_________學系/研究所_________研究生所提之論文

____ 係由本

（題　　　　目）

人指導撰述，同意提付審查。

指導教授____________________(簽章)

____年____月____日

國立中央大學博士班研究生

論 文 口 試 委 員 審 定 書

____________學系/研究所_________研究生所提之論文

____

經本委員會審議，認定符合博士資格標準。

學位考試委員會召集人 __________________________

委　　　　　　　　員 __________________________

____

____

____

中 華 民 國　　　年　　　月　　　日

Contents

List of Figures

List of Tables

1. Introduction

According to Hindu cosmological mythology, ancient people believe that a giant turtle bears the world on its back. Even after we stepped onto the moon at 1969, there are still plenty that we cannot explain. In the novel Lord of the Rings, the author named the path between hobbits as Mordor, which is also the name of the dark area on Pluto's moon, Charon. Recently, Mission New Horizons retrieved valuable data about Charon and Pluto. This thesis aimed to investigate the chemistry of VUV and EUV irradiations on CH_4+NH_3 ice mixtures, which is possibly the main compositions to form the red polar cap on Charon in figure 1.1.

According to Infrared (IR) spectroscopy, surface of Charon is a mixture of 90 % H_2O and 10 % tholin at millimetre depth. The main component which forms the dark red cap (tholin) is cold-trapped methane from Pluto's atmosphere ejecta [3]. The second possible component is ammonia. Since ammonia hydrate can be observed by earth-based telescopes [4]. Also in far IR spectrum taken by LEISA camera on the New Horizons, concentrated ammonia is found on Organa crater (figure 1.2) and throughout Charon (figure 1.3) [2]. The third component is methane. The presence of nitrogen and other ejecta from Pluto are neglected in this thesis because according to the model of Hoey et al.[3] (figure 1.4), during New horizons' approach, 98 % of the arrived ejecta is CH_4. CH_4 remains undetectable by infra-red spectroscopy nor VUV spectroscopy.

Ly-α appears to be the largest source in the dark side of Charon, with attributions from both solar occultation (70 %) and resonance scattering by atomic hydrogen flow (30 %) in the solar system at flux 3.5×10^7 photons cm^{-2} s^{-1} onto the winter pole of Charon [1]. The flux is 50 % larger than expected before Mission New Horizons [5]. CH_4

Figure 1.1: An overlapped figure of Charon taken from 3 filters of MVIC camera and LORRI camera to show topological details. (quoted from [1])

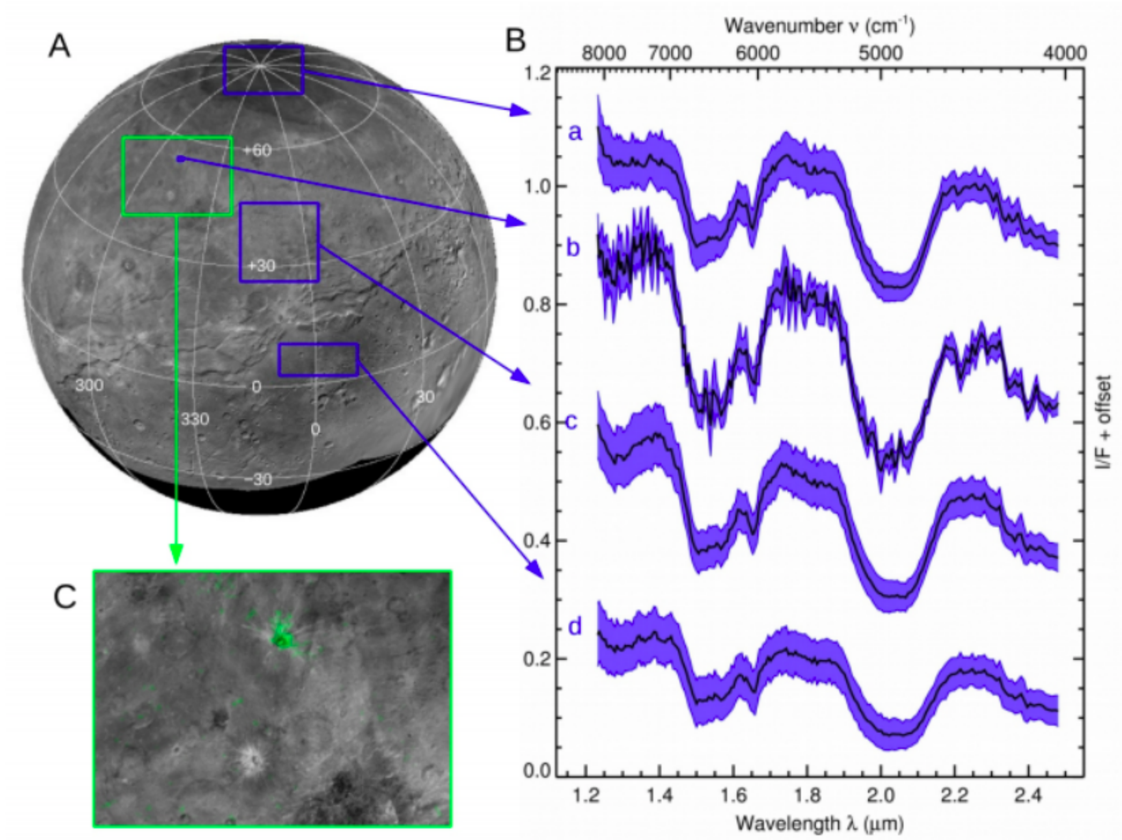

Figure 1.2: The 2.2μm absorption taken by LEISA camera colored as green on the topology shown by LORRI camera (A) and the spectra at 4 positions with b taken near organa crater.(quoted from [2])

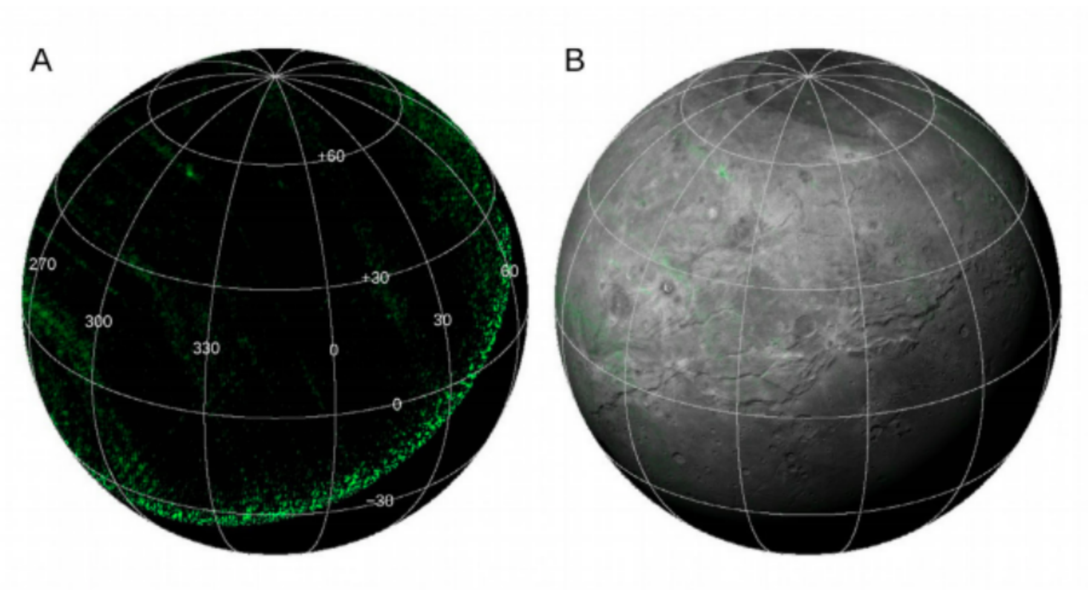

Figure 1.3: The 2.2 μ m absorption taken by LEISA camera with ammonia marked as green (A) and the topology shown by LORRI camera (B).(quoted from [2])

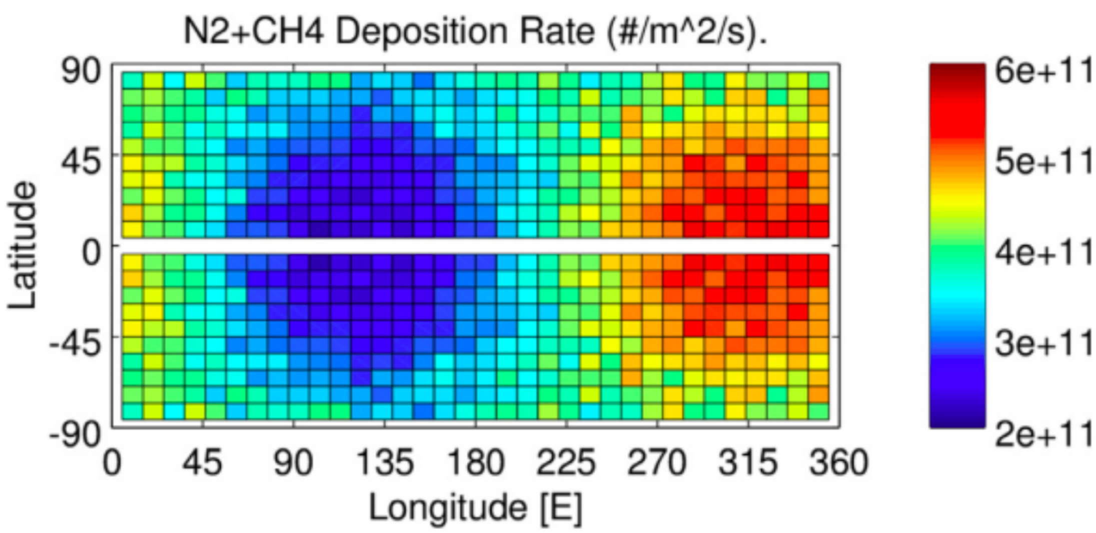

Figure 1.4: The simulation of N_2 and CH_4 model assuming all arrived molecules will stick onto the surface of Charon. Among the deposition rate, 98 % of them are CH_4 because CH_4 is lighter and preferentially escapes. The molar fraction of CH_4 increase from hypothesized 0.44 % to 42 % in the exobase of Pluto.(quoted from [3])

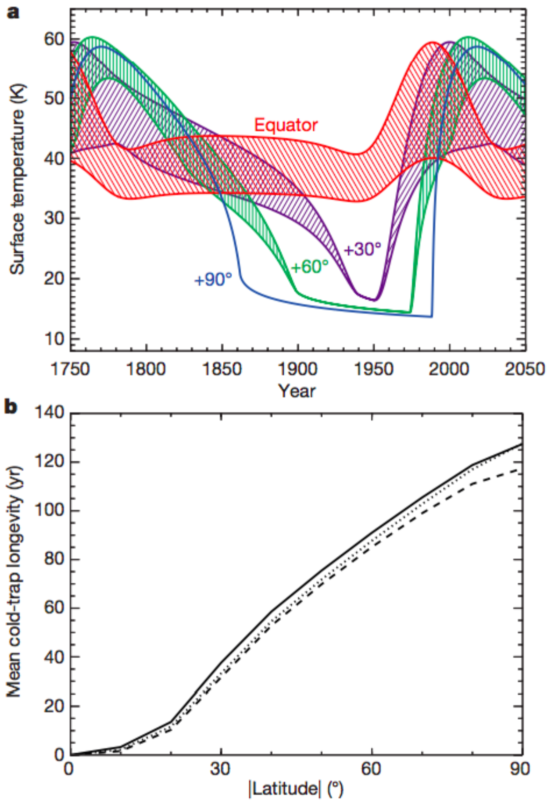

Figure 1.5: The temperature of Charon with thermal inertia 10 J m^{-2} K^{-1} $s^{-1/2}$ in 1750 to 2050 Earth years (a) and longest time the Latitude is under 25 K with the model averaged for 3 Myr with 2.5 (solid) 10 (dotted) and 40 (dashed) J m^{-2} K^{-1} $s^{-1/2}$ (b).(quoted from [1])

deposits at temperature below 25 K at pressure 7.4×10^{-14} torr. The time for depositing CH_4 is 2 times longer at the pole (130 earth years) than at 45° lattitude according to the thermal model of Grundy et al. [1] (figure 1.5). In order to understand the formation of tholin at different latitudes of Charon, we performed VUV irradiation on CH_4+NH_3 experiments with different ratios (including 3:2, 1:5, 1:10 and 1:20 for CH_4+NH_3 to simulate the conditions at different latitudes on Charon with base pressure 3×10^{-10} torr, simulating atmosphere on Charon at 15 K, which corresponds to temperature on Charon at winter times [1] in interstellar processing system (IPS) [6].

Apart from VUV irradiation, EUV irradiation also took part. VUV irradiation is believed to be the main process to convert CH_4 into heavier molecules which remained on the surface of Charon until the temperature of Charon become 60 K, at which methane evaporates from the ice. The ice is then further processed by EUV, solar wind, coronal mass ejections and interstellar pickup ions, etc to produce the tholin on Charon [1]. The EUV irradiation (>12.4 eV) is 8.7×10^{7} eV cm^{-2} s^{-1} at mean heliocentric distance 39 A.U. whereas VUV irradiation (Ly-α) is 1.9×10^{9} eV cm^{-2} s^{-1}[1]. In order to investigate the effectiveness of EUV to VUV irradiation, we kept temperature of CH_4+NH_3 (3:2 & 1:5) ice mixtures at 15 K and use the monochromatic 30.4 nm (He II) light provided by High flux beamline at National Synchrotron Radiation Research Centre (NSRRC) in Taiwan to irradiate the ice mixtures.

In this text, we will introduce the formation reaction mechanisms of CH_4+NH_3 ice mixtures in EUV and VUV irradiation, effectivness with electron irradiation experiments and a functional group comparison with tholin on Titan will be made. With these results, we will have a better understanding about Charon and some astrophysical implications will be presented in chapter 4.

2. Methods

2.1 Laboratory Astrophysics

To study the chemical reactivity in astrophysical environment experimentally, we conducted our experiments in Interstellar photoprocessing system (IPS) [6], an ultrahigh vacuum chamber with base pressure 3×10^{-10} torr and 14 K, corresponds to a density of 10^6 cm^{-3}, similar to dense cloud interiors. The system will be introduced in detail in section 2.1.1. To simulate the irradiation in interstellar environments, we use a micro-wave discharge hydrogen lamp (MDHL) and monochromatic extreme-ultraviolet irradiation (EUV) 30.4 nm to irradiate our ice mixtures, and they will be introduced in section 2.1.2 and 2.1.3 respectively. The experimental protocols will be elaborated in section 2.2. In order to better understand the physics behind, some basic theories of Infrared spectroscopy and concepts of chemical kinetics used in data analysis are included in section 2.3 and 2.4 respectively.

2.1.1 Experimental simulations by IPS system

We conducted our astrophysical simulations in Interstellar Photo Processing System (IPS) (figure 2.1). IPS consists in three systems: the main chamber, where our experiments take places; the detection system, where we collect our data; and a gasline system, where we prepare our samples.

The main system consists of an ultrahigh vacuum chamber equipped with a closed-cycle helium cryostat (CTI-M350). It is pumped by a turbo molecular pump, which is backed up by a scroll pump, and a non –evaporation getter pump. The getter pump is a powerful tool to adsorb residue gases inside the main chamber, with a larger surface area, H_2, CO and N_2 are adsorbed to obtain a better base pressure. After baking,

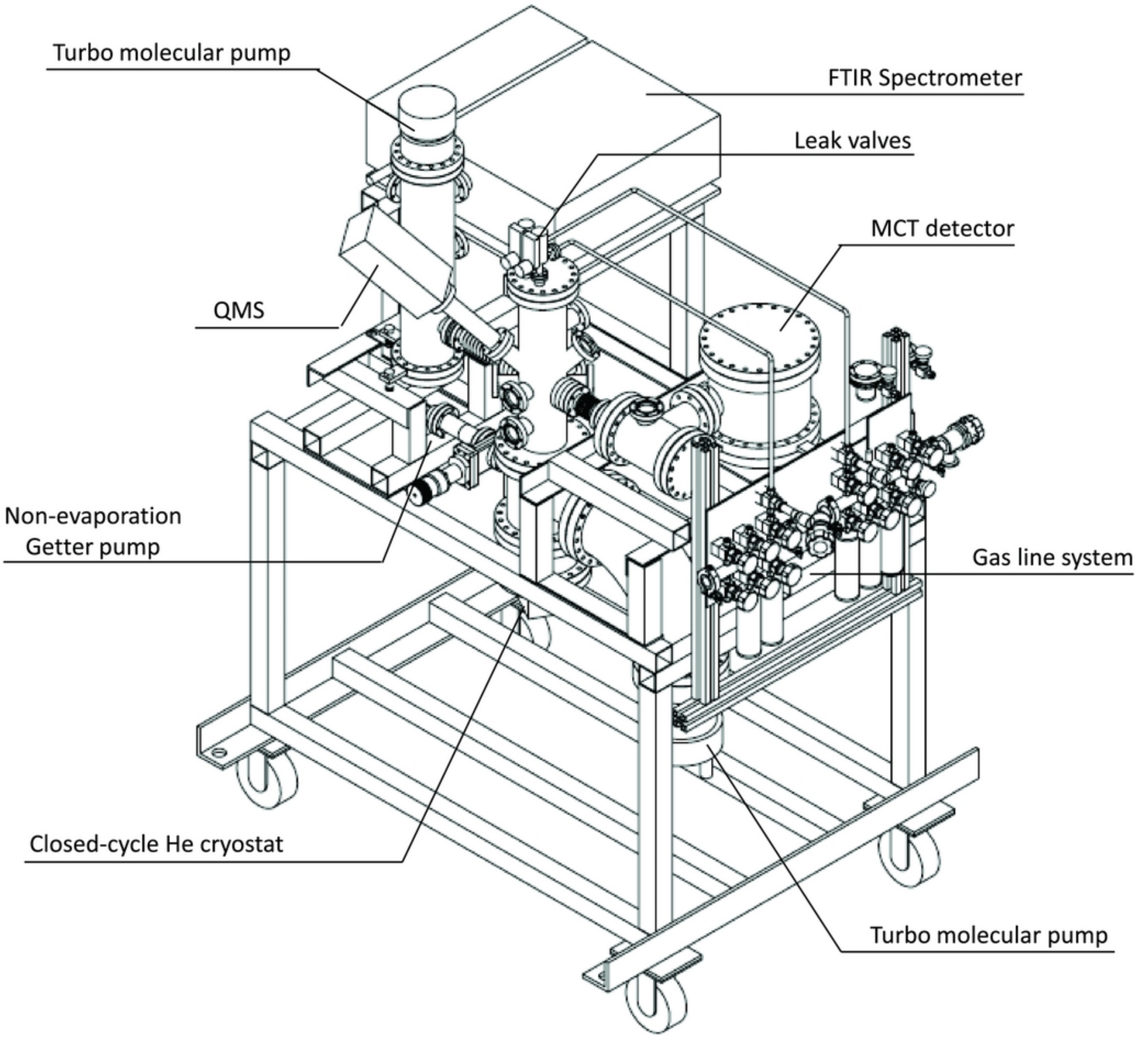

Figure 2.1: The schematic diagram of IPS system, mechanical pumps are not shown for clarity. (Quoted from Chen et al. 2014)

the base pressure of our main chamber can reach 1×10^{-10} torr at 14 K, monitored by a Granville-Phillips 370 Stabil-Ion gauge. This pressure can be used to demonstrate the dense cloud interior environments and star forming region. The substrate we have chosen is KBr, which can allow infra-red photons with 700 to 4000 cm^{-1} to penetrate. It is mounted by substrate holder made of oxygen-free copper, on the second stage of cold finger mounted on the tip of cryostat. Two silicon diodes and also a heater were placed onto the cold finger and one of the silicon diodes is near the substrate holder. They were connected to a temperature controller and PID system to achieve a warmup rate of 1K/min with an accuracy of 0.1 K.

The detection system consists in a mid-infrared Fourier transform spectrometer (mid-FTIR) (ABB FTLA2000-104) and a Quadrupole Mass Spectrometer (QMS). To prevent absorption bands of CO, CO_2 and H_2O gas in the atmosphere, the IR beam path was built inside vacuum, pumped by dry pump. The main chamber and the IR path are separated by ZnSe windows, which can allow infra-red penetration from 0.5 – 20 um with absorption less than 0.07 %. In this study, the infrared spectra are obtained with resolution of 4 cm^{-1} and averaged over 32 scans. The angle between the IR beam path and the substrate holder is 45 degrees. The QMS (MKS Microvision 2) consists of a controller and mechanical part sealed by a mounting flange in ultrahigh vacuum. It is mounted 10 cm from the substrate and run with a resolution 0.5 a.m.u. The Ionizer release 70 eV electron by filament and ionize incoming molecules to positive charged ions between anode grid and repeller. The ions were accelerated by focus plate and enters ion filter, which consists of four circular rods, with a combination of A.C and D.C. potential to sieve whole bandpass ions at millisecond timescale. The selected ions enter ion detector and are detected by either faraday cup and continuous dynode electron multiplier (CDEM) which can secondary multiply weak signals.

The samples are prepared in situ in our gasline system. It contains four stainless steel bottles with the same volume, which is used to determine relative proportion of the gas mixtures by their partial

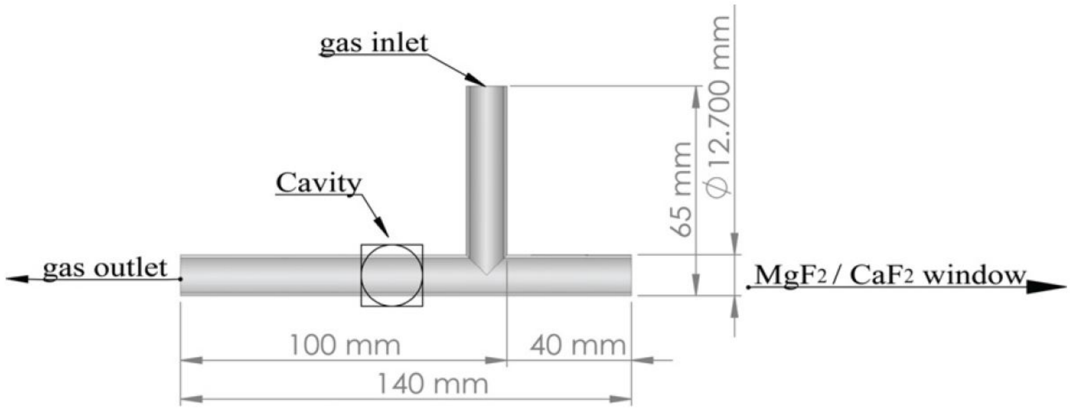

Figure 2.2: The cross-section of MDHL (T-type geometry) (Quoted from Chen et al. 2014).

pressures. The ammonia gas 99.99 % and methane 99.999 % are mixed with partial pressure measured by a Baratron with 0 - 100 torr range with a 0.25% accuracy. The background pressure of the gasline system is lower than 1×10^{-7} torr thank to a turbo molecular pump (Oerlikon Leybold TurboVac 151, capacity 145 liters s-1) backed up with an oil-sealed mechanical pump (Alcatel 2012A, capacity 450 $liters minute^{-1}$), equipped with an oil trap (molecular sieve type 13X). Water were bought from Merck which is LC-MS Grade and purified before use, by several freeze-pump-thaw cycles under vacuum.

2.1.2 Vacuum-UV source

In order to simulate the photoprocessing of vacuum ultraviolet (VUV) irradiation onto the interstellar ices and ices on planetary bodies, including KBOs, the ice mixtures are irradiated with a T-type Microwave-Discharged Hydrogen-flow lamp (MDHL). The molecular hydrogen with pressure 0.4 torr flows through the lamp with a support of a mechanical pump. Using a 2.4 GHz microwave generator and high voltage discharge, a low pressure plasma is produced in the Evenson cavity. Figure 2.2 shows a cross-section of T-type quartz tube; the middle part of the T-type quartz tube is being tunned by a ceramic rod that is called Evenson cavity. In order to measure the photon flux in situ, we use an 88 % transmittance nickel mesh with its photoelectric efficiency being obtained by high-flux beamline in National Synchrotron and a SXUV 100 photodiode calibrated by NIST. A MgF_2 window is

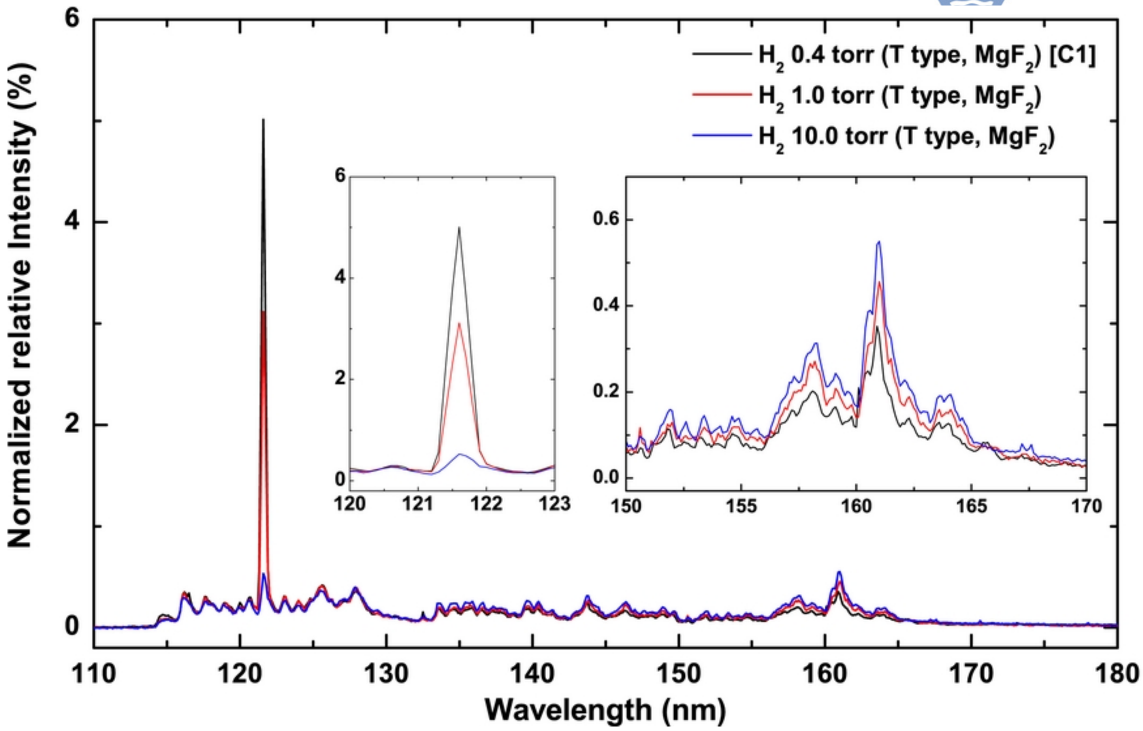

Figure 2.3: VUV spectra of MDHL (T-type geometry, 110-180 nm) with different H_2 pressure inside the lamp(Quoted from Chen et al. 2014).

placed between the lamp and the sample holder to prevent penetration of VUV photons with wavelength shorter than 114nm, leads to a cut off at 114nm. Figure 2.3 shows a VUV emission spectrum of a MDHL. It consists in Ly-α (121.6nm) and H_2 molecular emission in 110-180 nm range. Chen et al. (2014) showed that the spectral characteristics of the VUV light emitted in this range depends on the gas type (mixture of H_2 with He or Ar etc), pressure of H_2 and lamp geometry. Throughout those configurations stated there, we adopted 0.4 torr molecular hydrogen and T-type MDHL that produces VUV irradiation at 114-170 nm with 19.1 % of Ly-α and a mean photon energy of 9.27 eV. The photon flux is 6.4×10^{13} photons $cm^{-2}s^{-1}$ at sample position.

2.1.3 Extreme EUV source

To simulate the solar EUV irradiation reflected by IPM on both Charon and interstellar ices, we use the HF-CGM high – flux beam line of the National Synchrotron Radiation Research Center in Hsinchu, Taiwan. It provides a continuum EUV to VUV photons from 4 to 40 eV. The continuum is separated into monochromatic 30.4nm photons with a six-meter cylindrical grating monochrometer with an incident angle of 70 degrees. With the help of a movable entrance slit and movable curved exit slit, the energy resolving power can reach around 3×10^4 at 40 eV for grating 1600 l/mm with both slits movable and set opening to 10 μm [7]. Similar to VUV irradiation provided by MDHL, the light intensity was monitored by the same nickel mesh with photoelectric efficiency obtained by SXUV 100 photodiode calibrated by NIST. With the known photoelectric efficiency, the flux of monochromatic 30.4nm is measured to be 2.15×10^{14} photons $s^{-1}cm^{-2}$ with a spot size of 1 cm

2.2 Experimental Protocol

In this section, we will briefly introduce the procedures of how we performed our experiments. It is divided into four parts, preparation and cooling, deposition, irradiation and warmup.

Preparation of experiments and cooling

Before any of experiment is done, we bake our system at 100 oC for 48 hours to reduce the contamination of water and residue gases as much as possible. It was cooled to room temperature that the background pressure can reach routinely at 1×10^{-10} torr. The gasline were connected with the regulators of the gas tanks and bake to 100 ^oC and pumped by molecularturbo pump for two days before any experiment were done. Also, The water sample has been freeze thaw several times by liquid nitrogen until there is no pressure increase recorded by baratron when water is freezed. Before cooling the substrate to cryogenic temperature, we took an IR spectrum and started the monitoring of residue gases by QMS in order to compare the residue molecules and to verify any possible contaminations in the main chamber. We then start the cooling process thanks to the closed-cycle He cryostat.

Deposition

The gas mixtures are pre-mixed in our gasline system introduced in section 2.1.1. We used a leak valve to condense the gas from the stainless steel bottles onto pre-cooled KBr substrate at 14 K, which monitored by Fourier transformed Infra-red spectroscopy (FTIR) and

Quadrupole mass spectrometer (QMS) during deposition. The pressure of deposition is fixed to 1×10^{-8} torr that the deposition rate is $4 \times 10^{16} moleculescm^{-2}min^{-1}$. After deposition, we placed the ice mixture at 14 K for 60 minutes and to allow pumping of residue gas, until pressure of the main chamber reduce back to its base pressure to simulate the interstellar environment before irradiation.

Photon Irradiation

The total irradiation time is 270 to 450 minutes depend on experiment configurations; with time intervals varies from 2 to 30 minutes. After each irradiation, we waited for 10 minutes allowing pumping out of the photodesorpted gas molecules. During irradiation, the photon flux is monitored by a nickel mesh. After Irradiation, we place the sample for 30 minutes to observe if any thermal reaction was conducted.

Warmup

We use 1 K/min to warmup the substrate to 300 K to demonstrate effects of a new born star nearby an interstellar cloud. During warmup, we record the QMS from 1 to 100 a.m.u. to observe if there are low quantity of higher mass product formed during irradiation.

2.3 Infra-red spectroscopy and the Beer's Law

We used infra-red spectroscopy extensively in chapter 3 and 4, it is a powerful tool in studying molecular interactions during irradiation and warmup. We choose infra-red rather than Ramen spectroscopy because infra-red has lower energy that it would not change the structure of the ice mixture nor breaking any of the bonds. With different vibration modes, the energy absorbed by molecules are quantized. With the energy of absorption bands in infra-red spectrum, we may identify the functional group of the species. To simply classify, molecules can have, from less energetic, translational, rotational and vibrational motions. Generally, vibrational motions can be divided into stretching and bending. Stretching needs more energy than bending. For stretching, there exist Symmetric and Asymmetric stretching, while bending can be

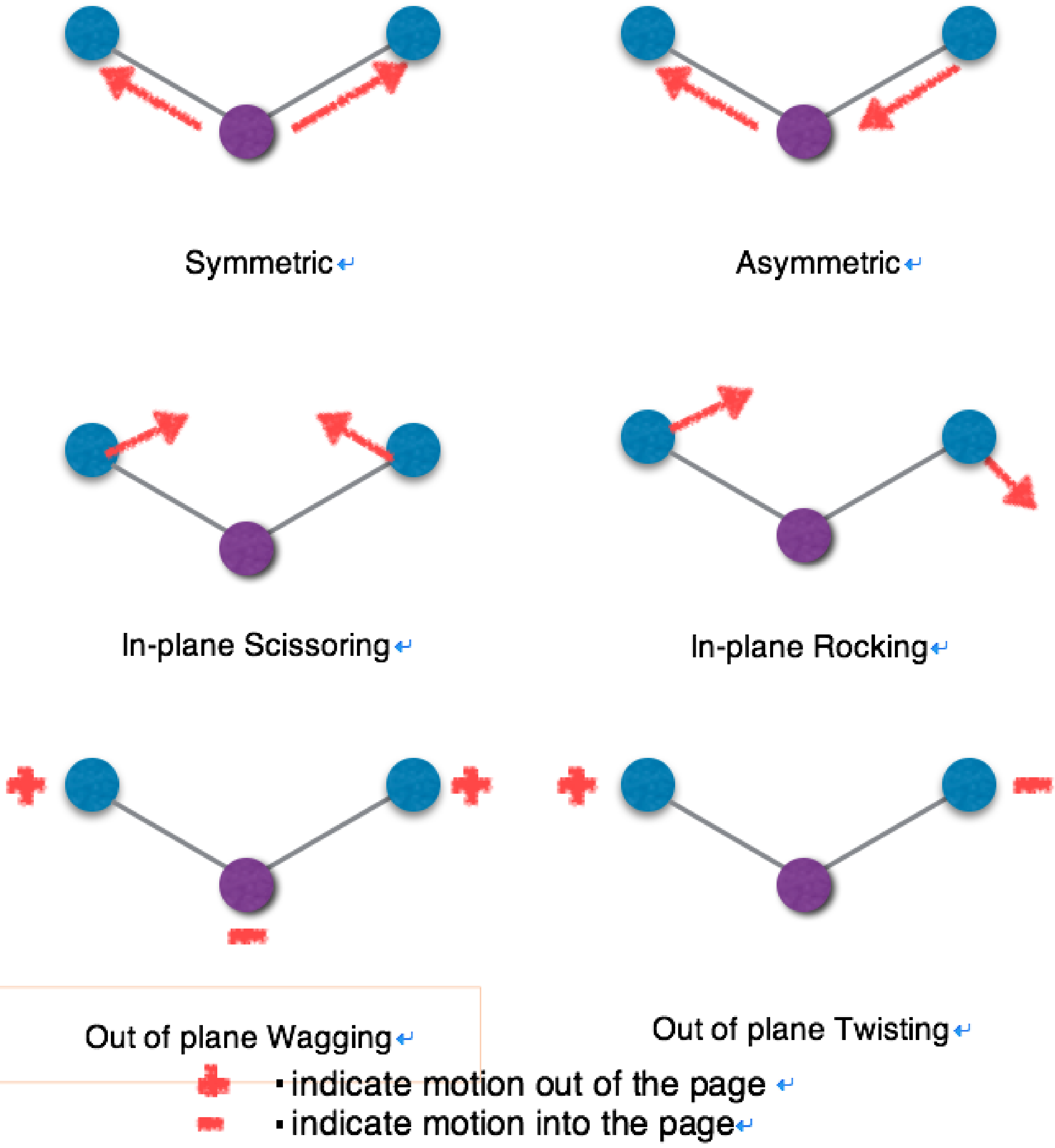

Figure 2.4: Different vibrational modes of a three atom molecule.

divided into In-plane Scissoring, rocking and out of plane Wagging and Twisting (Figure 2.4).

By Beer's Law, we may calculate the column density of the molecule with its functional groups, which are used to plot figures in chapter 3 and 4. Beer Lambert's Law suggest that when light passes through a medium, amount of light absorbed is proportional to density and path length of the medium. Assume the known intensity beam $I_0(\nu)$ passes through the medium and beam intensity become $I(\nu)$. The transmittance $T(\nu)$ is defined by equation 2.1.

$$T(\nu) = \frac{I(\nu)}{I_0(\nu)} \tag{2.1}$$

Also, the absorbance $a(\nu)$ is defined by equation 2.2.

$$a(\nu) = -\ln T(\nu) = -\ln \frac{I(\nu)}{I_0(\nu)} = nl\sigma(\nu) \tag{2.2}$$

where n is number density (molecules/cm^3), l is the path length (cm), $\sigma(\nu)$ is the cross-section (cm^2/molecule) of corresponding frequency ν. This equation is known as Lambert Beer's Law.

As the ice mixture in our thesis are at 14K, the peaks of absorbance are often a broadband due to coupling between neighbor molecules. Therefore, we can integrate the whole band of the peak equation 2.2 with respect to frequency and use the absorbance strength (A value) in literatures to calculate the column densities N of the ices by equation 2.3.

$$N = \frac{\int a(\nu)\mathrm{d}\nu}{A(\nu)} \tag{2.3}$$

where N is the column density (molecule cm^{-2}), $A(\nu)$ is the absorbance strength (cm molecule^{-1}).

2.4 Reaction Rate Laws

In this section, we will introduce rate reaction of a consecutive reaction and the concept of pseudo first order which we used to fit our reaction product against irradiation time. The rate of a chemical reaction is the relation between change in concentration of a substance per unit of time. i.e. For a balanced chemical reaction, A $\rightarrow$ 2B, the rate of reaction is $-\frac{\Delta[A]}{\Delta t}$. The formation rate of B is 2 times destruction rate of A.

To determine the order of a reaction, we can only determine it experimentally. For a zero order reaction, the rate is not depending on any reactant that it is a constant. The rate $= -\frac{\Delta[R]}{\Delta t} = k[R]^0$. By calculus, $[R]_0 - [R]_t = kt$.

For a first order reaction, rate $= -\frac{\Delta[R]}{\Delta t} = k[R]$. By calculus, $\ln[R]_t = -kt + \ln[R]_0$.

For a second order reaction, rate $= -\frac{\Delta[R]}{\Delta t} = k[R]^2$. By calculus, $\frac{1}{[R]_t} - \frac{1}{[R]_0} = kt$.

Hence, if we get a straight line in a time versus concentration plot ,it is a zeroth order reaction, similarly, in first order reactions, we get proportional relationships in time versus $\ln[R]$.

In a reaction with one reactant in excess, the rate of reaction is called pseudo first order reaction where pseudo means pretended. For A+B $\rightarrow$ C, rate $= k[A][B]$. As $[B]_0 \gg [A]_0$, change of $[B]$ is negligible that $[B] \sim [B]_0$. Therefore, $[B]$ is assumed to be a constant and included in the rate constant k.

For a consecutive reaction equation, which we used to fit our data points, where A $\rightarrow$ B $\rightarrow$ C that the produced product will not convert back as reactant. A simple example is radioactive decay. At $t = 0$, $[A] = [A]_0$, $[B] = 0$, $[C] = 0$ and at all times, $[A] + [B] + [C] = [A]_0$. The rate equations are as follows:

$$-\frac{\Delta[A]}{\Delta t} = k_1[A] \tag{2.4}$$

$$-\frac{\Delta[B]}{\Delta t} = k_1[A] - k_2[B] \tag{2.5}$$

$$-\frac{\Delta[C]}{\Delta t} = k_2[B] \tag{2.6}$$

By equation 2.4, we get

$$[A] = [A]_0 e^{-k_1 t} \tag{2.7}$$

By substituting equation 2.7 into equation 2.5, we get

$$-\frac{\Delta[B]}{\Delta t} + k_2[B] = k_1[A]_0 e^{-k_1 t} \tag{2.8}$$

After solving the differential equation 2.8 , we get

$$[B] = \frac{k_1}{k_2 - k_1}(e^{-k_1 t} - e^{-k_2 t})[A]_0 \tag{2.9}$$

Finally, since $[C] = [A]_0 - [B] - [A]$, by equation 2.7 and 2.9, we get

$$[C] = \left(1 + \frac{k_1 e^{-k_2 t} - k_2 e^{-k_1 t}}{k_2 - k_1}\right)[A]_0 \tag{2.10}$$

3. Results and Discussions

According to the New Horizons team [1], CH_4 from Pluto may accumulate by cold-trapping, onto the surface of Charon. The amount of CH_4 varies along the surface of Charon because it depends on the length of time the temperature is below 25 K which in turns depends on diurnal motion and thermal inertia of Charon. With an axis tilted by 112 degrees from the ecliptic, higher concentration of CH_4 will be accumulated at the pole (see chapter 1 for details). In this chapter, we will investigate the following by infra-red spectroscopy: 1. The photo products produced by different concentration ratios of methane to ammonia, 2. the photo products produced by different photo sources (i.e. EUV and VUV) 3. the reaction mechanisms of each main products and 4. the functional group of tholin formed by irradiation of VUV, EUV on different configurations of CH_4+NH_3 ice mixtures (the result is compared with the residues on Titan produced by Imanaka et al. [8]).

3.1 The infra-red spectrums and peaks identification

We scanned the IR spectrum before and after deposition and plotted the plot the corresponding absorbance of the ice mixtures. Figure 3.1 is a plot of the absorbance of the CH_4+NH_3 ice mixtures in different concentration ratios: 1:20, 1:10, 1:5 and 3:2 (arrangedfrom top to bottom). We labelled the peaks used in column density calculation by dotted lines in the graph. Main products we have detected are C_2H_6, CN^- and C_3H_8. The peak positions for substance identification are listed in Table 3.1. After identification of the products, we will look into each main products individually.

To calculate the column density, we integrate the area under graph and divided by the absorption strength presented in table 3.2. We aware

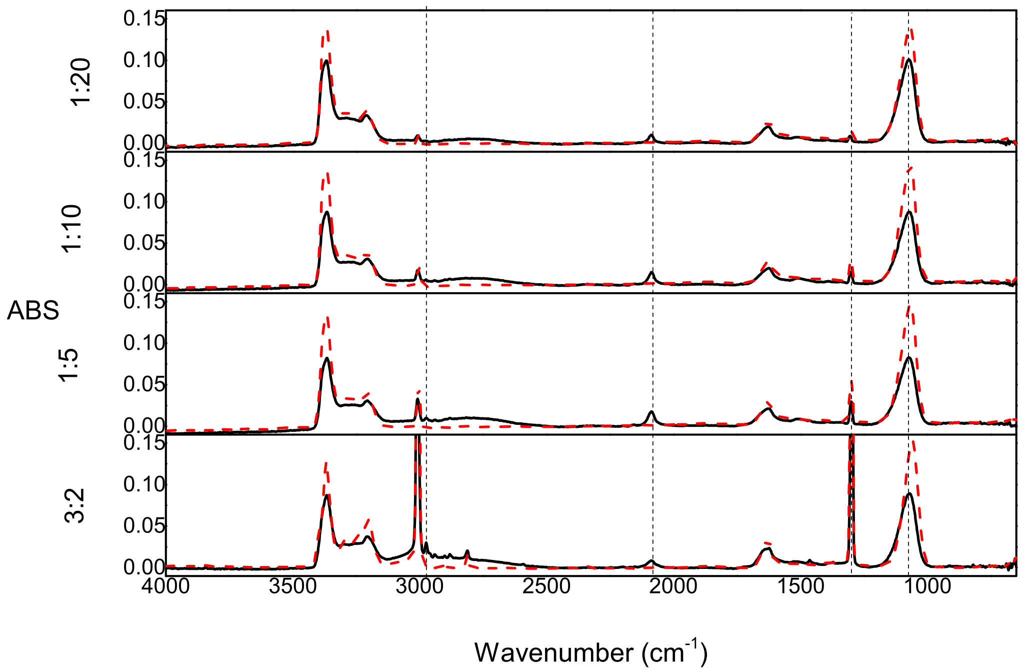

Figure 3.1: The the infra-red spectrum of CH_4 + NH_3 ice mixtures before irradiation (dashed) and VUV irradiated ice mixtures provided by MDHL.

Table 3.1: The peak positions of identified substances after irradiation in different configurations of ice mixtures.

Literture assignments		CH_4+NH_3 ratio (MDHL)				
Wavenumber (cm^{-1})	Carrier	1:5 (cm^{-1})	1:10 (cm^{-1})	1:20 (cm^{-1})	3:2 (cm^{-1})	Ref.
3375	ν_3 (NH_3)	3366	3366	3369	3367	1
3290	$2\nu_4$ (NH_3)	-	-	-	-	1
3210	ν_1 (NH_3)	3207	3208	3210	3205	1
3011	ν_3 (CH_4)	-	-	-	-	2
2972	ν_{10} (C_2H_6)	2975	-	-	2975	3
2960	C_3H_8	-	-	-	2960	7
2941	$\nu_8 + \nu_1 1$ (C_2H_6)	2940	-	-	2940	3
2904	ν_1 (CH_4)	2901	-	-	2901	5
2879	ν_5 (C_2H_6)	2882	2883	-	2882	3
2814	$\nu_2 + \nu_4$ (CH_4)	-	-	-	2815	5
2083	ν (CN^-)	2088	2087	2088	2088	2
1625	ν_4 (NH_3)	1625	1625	1626	1631	1
1514	δ (NH_2)	1509	1507	1505	1511	6
1465-1440	deform CH_2 scissor	1461	-	-	1463	3,4
1390-1370	CH_3 sym deform	1394	1394	1394	1372	4
1298	ν_4 (CH_4)	1301	1302	1305	1299	2
1075	ν_2 (NH_3)	1073	1072	1072	1072	1
820	$\nu_1 2$ (C_2H_6)	-	-	-	820	3

Reference: 1. Bossa et al. 2008 [9] 2. Moore and Hudson 2003 [10] 3. Kim et al. 2010 [11] 4. Socrates 2001 [12] 5. Bennet and Kaiser 2007 [13] 6. Zheng et al. 2008 [14] 7. Hudson and Moore 2004 [15] that there is an average error in absorption strengths of no more than 10 % when the pure ice is diluted in N_2 and H_2O [16]. In our case, absorption strengths changes after CH_4 and NH_3 are mixed. For example, according to d' Hendecourt and Allamandola [17], the band of NH_3 located at 1070 cm^{-1} would not change much (from 1.1×10^{-17} to 1.2×10^{-17}) when excess water is added to pure NH_3. For the case of CN^-, we know that CN^- has a bond order =3 from its molecular orbitals. CN^- which is different from CN (bond order 2.5). CN stretching is very sensitive to the matrix environment. It can change by factor of 2 in amino acetonitrile and H_2O (1:3) [18]. However, CN is not inspected in this chapter. Therefore, we are justified to use the same absorption strength throughout our discussion to estimate the column density of each species and how the absorption area changes with concentration ratios of ice mixtures and photon energy. Here, we adopt the absorption strengths stated in Table 3.2

Table 3.2: The strength of absorbance adopted in this thesis measured in literatures of pure ice samples

Wavenumber (cm^{-1})	Assignment	Vibration	FWHM	A value ($\times 10^{-17}$)	Reference
2976	C_2H_6	$-CH_3$	-	1.05	2
2960	C_3H_8	$-CH_2-$	-	2.58	2
2086	CN^-	CN	-	1.8	3
1297	CH_4	CH deformation	8	0.61	1
1070	NH_3	"umbrella mode"	68	1.7	1

Reference: 1. d'Hendecourt and Allamandola (1986)[17] 2. Moore and Hudson (1998)[19] 3. Noble et al. (2013) [20]

3.2 Reaction mechanisms

3.2.1 C_2H_6

The assignment of C_2H_6 is confirmed by several bands listed in table 3.1. Figure 3.2 is a zoomed view of figure 3.1. The absorption peak located at 2075 cm^{-1} corresponds to the strongest vibration of C_2H_6. The formation of C_2H_6 in astrophysical environment is mainly through a combination with 2 CH_3 radicals [21]:

$$CH_4 + hv \rightarrow CH_3 \tag{3.1}$$

$$2CH_3 \rightarrow C_2H_6 \tag{3.2}$$

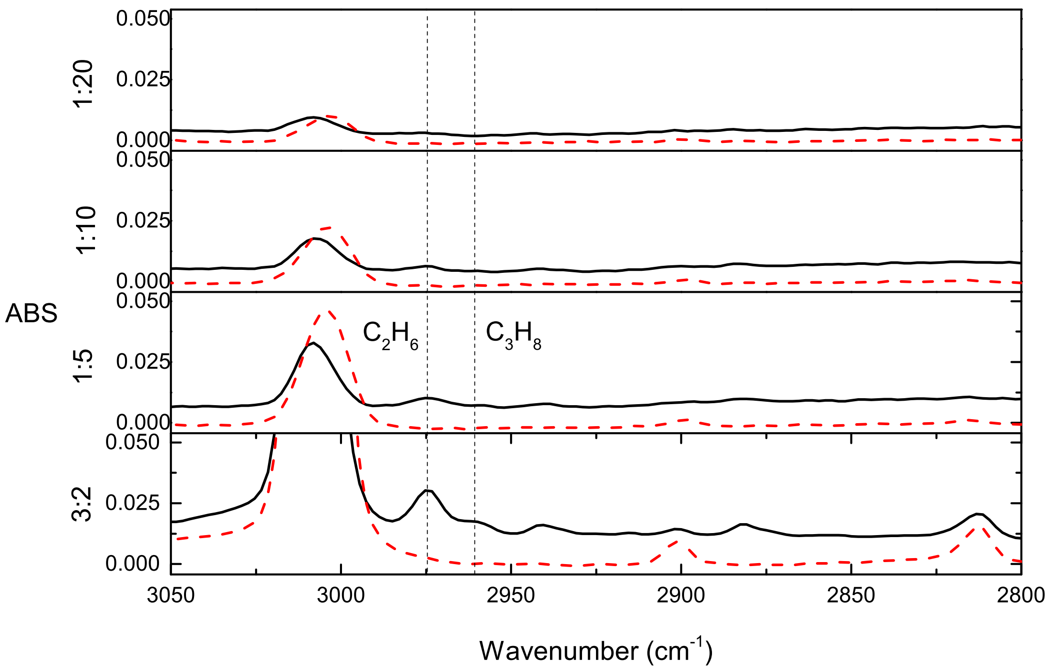

Figure 3.2: The the infra-red spectrum of CH_4 + NH_3 ice mixtures of C_2H_6 and C_3H_8 before irradiation (dashed) and VUV irradiated ice mixtures provided by MDHL.

The energy required to produce 1 CH_3 radical from CH_4 is 4.42 eV. Recombination of 2 CH_3 radicals to form C_2H_6 releases 3.74 eV. The process in 3.2 is a no-barrier exothermic process. Note that C_2H_6 is not detected in CH_4 to NH_3=1:20 ice mixtures. Figure 3.3 shows the temporal formation column density of C_2H_6 in different configurations of irradiated ice mixtures. As the formation only depends on CH_4, we may use first order kinetics equation to fit the column density versus photon dose.

$$[A] = [A]_0(1 - e^{-k_1 t}) \tag{3.3}$$

The fitting results are shown in table 3.3.

Table 3.3: The fitting results of C_2H_6 by $[C_2H_6]$=$[C_2H_6](1 - e^{-k_1 t})$

Ratio of CH_4+NH_3	A (x10^{15} molecules cm^{-2})	k (x10^{-17} photon^{-1})
1:10	2.90 ± 1.25	0.92 ± 0.15
1:5	4.16 ± 0.28	2.28 ± 0.28
3:2	19.2 ± 0.15	5.28 ± 0.25

From table 3.3, the production rate is nearly proportional to the

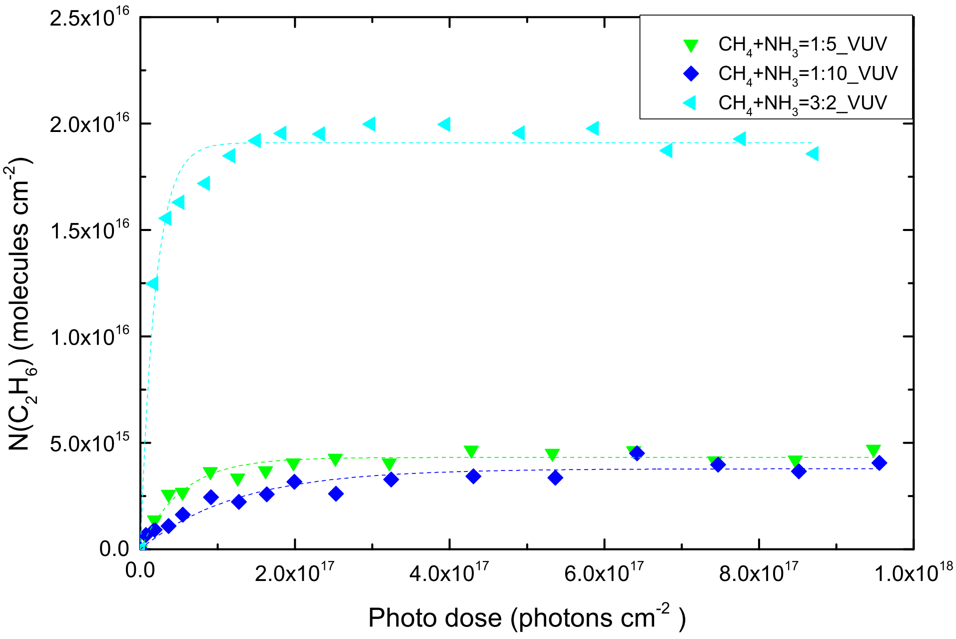

Figure 3.3: The column density of C2H6 during CH4 + NH3 ice mixtures irradiated by MDHL.

initial CH_4 concentration.

3.2.2 C_3H_8

The peak positioned at 2960 cm^{-1} belongs to –CH_2- so we assigned that as C_3H_8, as the shortest carbon chain. The signal to noise ratio in CH_4+NH_3 = 1:10 is poor that we can not quantize the amount of C_3H_8 (figure 3.2).

It is a secondary product formed by a combination of either C_2H_6 + CH_2 (equation 3.4)or C_2H_4 + CH_4 (equation 3.5).

$$C_2H_6 + CH_2 \rightarrow C_3H_8 \tag{3.4}$$

$$C_2H_4 + CH_4 \rightarrow C_3H_8 \tag{3.5}$$

By modern peak fitting method, we deconvoluted the overlapped C_2H_6 and C_3H_8 into two gaussians.

3.2.3 CN^-

From infra-red absorption spectrum (figure 3.4) and their positions, we assigned the peak 2086 cm^{-1} to CN^- but not a combination of HCN and CN^-. The assignment is based on a absence in CN bending mode at

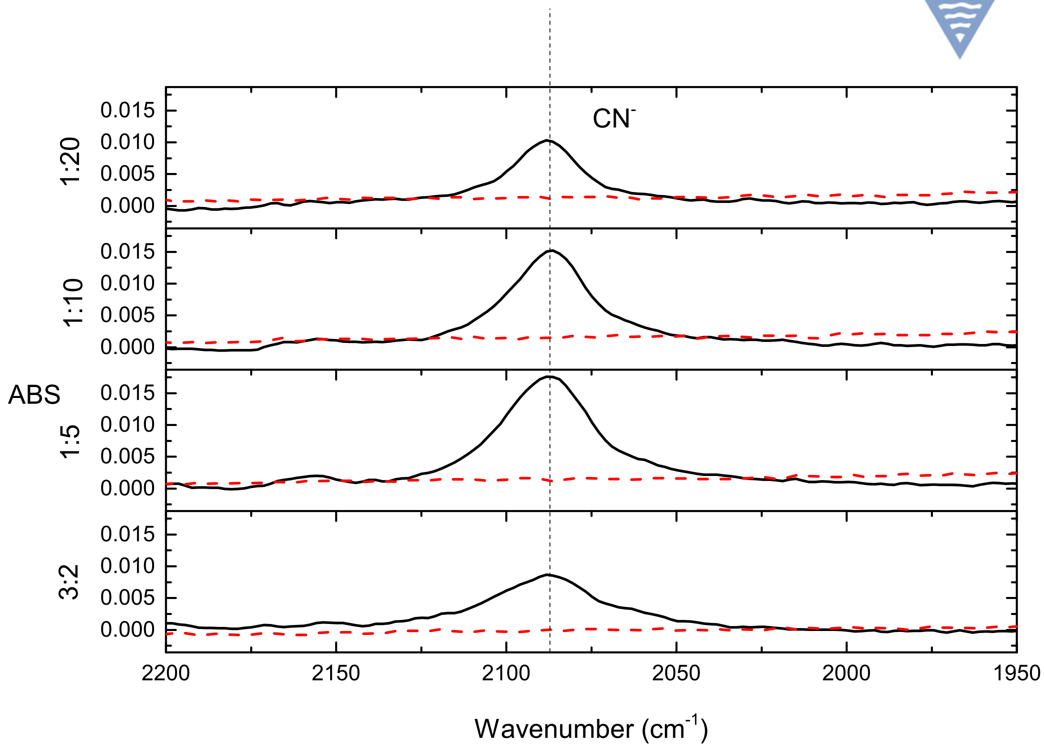

Figure 3.4: The infra-red spectrum of CH_4 + NH_3 ice mixtures of C_2H_6 and C_3H_8 before irradiation (dashed) and VUV irradiated ice mixtures provided by MDHL.

848 cm^{-1}. In the case CH_4 + NH_3 = 3:2, we may observe a peak located at 820 cm^{-1}, which is with a FWHM half of HCN and it is eliminated at 50 K during the warm-up phase. Since 50 K is the desorbing temperature of C_2H_6 and the peak position is the close to v12 mode of C_2H_6, we believe that the 820 cm^{-1} peak is contributed by C_2H_6. Therefore, we may assign our peak located at 2086 cm^{-1} as purely CN^-.

The formation mechanism of CN^- at low temperature was first suggested by Kim and Kaiser [22] to be two step reaction mechanism with methylamine as intermediate. CH_4 and NH_3 irradiated by photon to become CH_3 and NH_2 radical (figure 3.5, followed by propagation and recombination of radicals becoming CH_3NH_2 and dehydrogenation and acid-base reaction to form CN^-. Although Kim and Kaiser [22] used 1.5 keV electron as energy source to simulate the cosmic ray induced photochemistry, this formation mechanism also applies in our photon irradiation experiments because we can also detect the methylamine

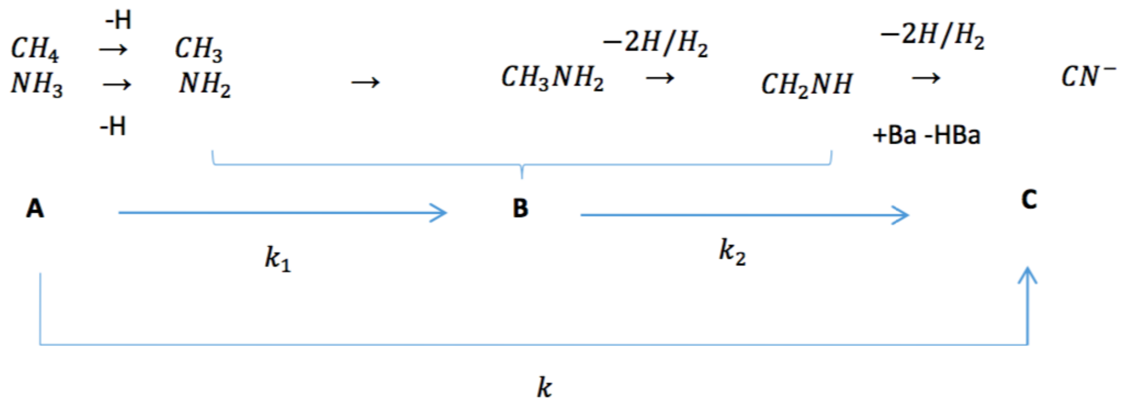

Figure 3.5: The formation mechanism of CN^- proposed by Kim and Kaiser(2011).

during our warm-up phase. The ion fragment with m/z=31 is assigned as $CH_3NH_2{}^+$ and detectable in all ratios of our CH_4+NH_3 experiments (figure 3.6).

By the deviation performed in section 2.4, we have a rate equation for consecutive reactions 2.10. With one of the reactant larger than another, we applied the pseudo first order assumption. With equation 2.10, we fitted the formation of CN^- (figure 3.7)and found that one of the rate constant is always larger than the other in all of the ratios. The fitting results are averaged by more than two experiments and are shown in table 3.6.The results of Kim and Kaiser is also listed into the table, they could observe a two-step reaction mechanism in production of CN^- in CH_4+NH_3 (3:1) experiments with electron current 0.1 μA. However, when they increased the electron flux to 1 μA for irradiation $C_nH_{2n+2(n=1-6)}$ and NH_3 ice mixtures, they also observed a one-step reaction mechanism.

Table 3.4: The fitting results of CN^- by equation 2.10

Ratio of CH_4+NH_3	A (x10^{16} molecules cm^{-2})	k_1 (x10^{-18} $photon^{-1}$)	k_2 ($photon^{-1}$)
1:20	4.75 ± 0.40	0.70 ± 0.09	>1
1:10	4.51 ± 0.18	1.33 ± 0.13	>1
1:5	4.61 ± 0.18	1.93 ± 0.19	>1
3:2	2.24 ± 0.03	8.21 ± 0.70	>1

A represents the amount of CN^- we may obtain when irradiated the ice for infinitely long.

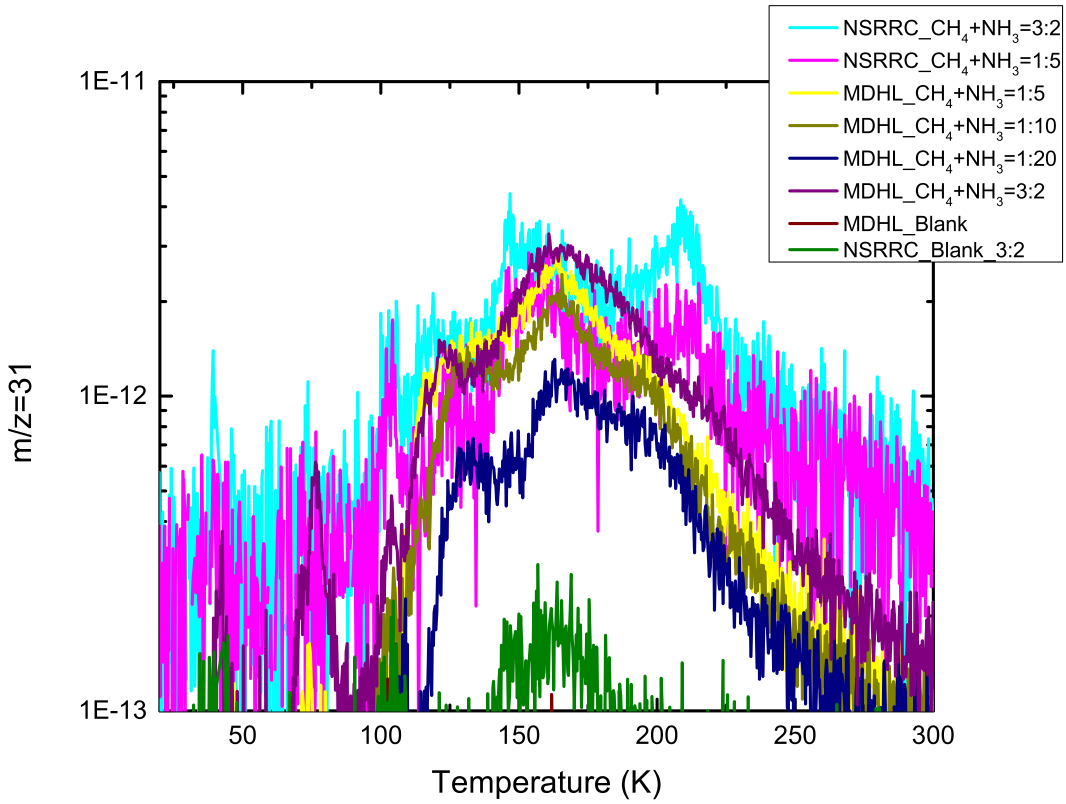

Figure 3.6: The m/z=31 detected by QMS during warm-up with heating rate 1 K/min in different configurations of ice mixtures.

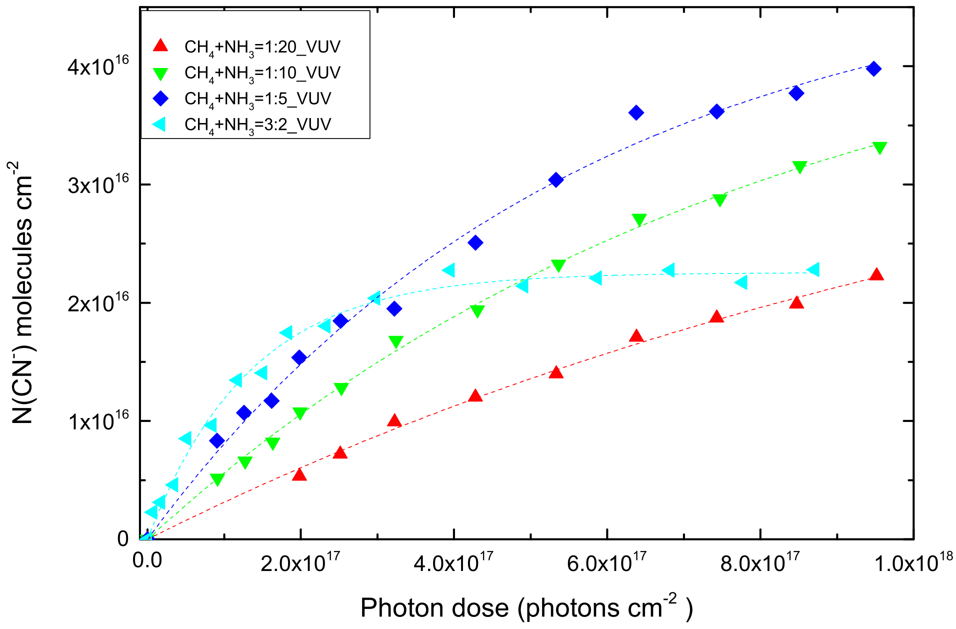

Figure 3.7: The column density of CN^- accumulated when different configurations of $CH_4 + NH_3$ ice mixtures are irradiated by VUV photons provided by MDHL. The dotted lines are fits of column densities by equation 2.10.

3.3 The Concentration Effect in formation of Cyanide ions and Ethane

3.3.1 Cyanide ion

From table 3.6, we may observe that the rate k_1 is nearly proportional to the concentration of CH_4. As CH_4 to NH_3 ratio increases, more CH_4 are involved in CH_3 radical formation, thus there are more CH_3 radicals to produce CH_3NH_2 intermediates.

In CH_4 to NH_3 =3:2 ice mixtures, A is about half of that of the other ratios. The reduction is mainly because NH_2 (forming CH_3NH_2) has a competing relationship with CH_2, CH_3 and C_2H_4 radicals (forming C_2H_6 and C_3H_8). This competition supresses the production of intermediate CH_3NH_2, thus the formation of CN^-. Therefore, the yield of CN^- is the least in CH_4 to NH_3 ice mixture with ratio 3:2 while the yield of C_2H_6 is the greatest in the mixture with the same ratio(table 3.6), (table 3.3)

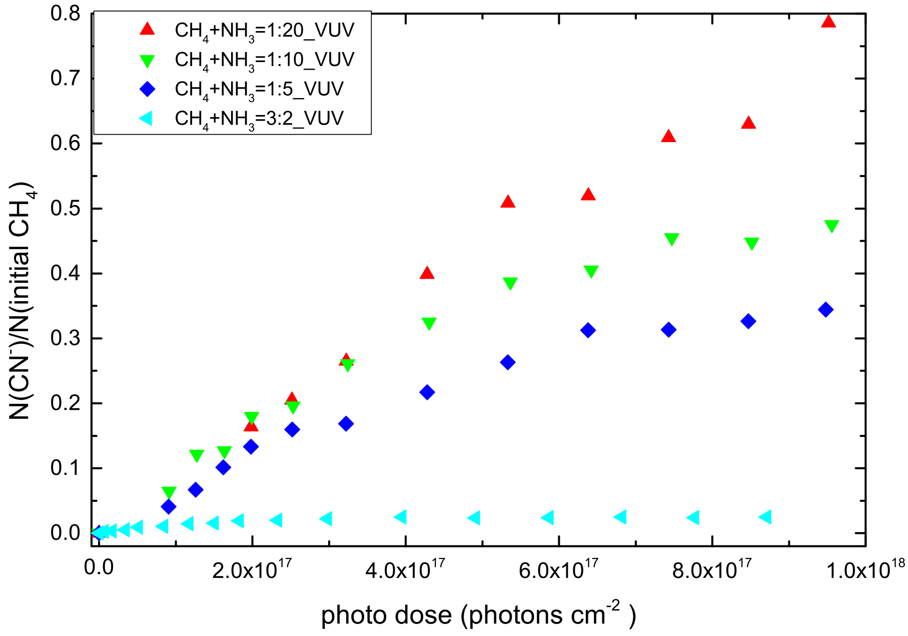

Figure 3.8: The column density of CN^- divided by initial CH_4 accumulated when different configurations of CH_4 + NH_3 ice mixtures are irradiated by VUV photons provided by MDHL.

Considering the normalized CN^- with respect to the initial CH_4(figure 3.8), the formation of CN^- is more efficient in low CH_4 concentration ice mixtures. At low CH_4 concentration, there are excess NH_3 which can aggregate mobile CH_3 radicals, preventing meeting another CH_3 radical or C_2H_4. Therefore the production of C_2H_6 is greatly suppressed and more CN^- will be produced.

3.3.2 Ethane

Considering the case of ratio of CN^- divided by C_2H_6,the formation of CN^- in ice mixtures with diluted CH_4 has more CN^- formed then C_2H_6. It is because ice mixtures with with higher concentrations in CH_4 is more effective for one CH_3 radical to combine with another CH_3 radical. On the contrast, CH_3 radicals formed in the ice mixtures with diluted CH_4 concentrations are aggregated by NH_3. Therefore, CN^- is less efficient to form in ice mixtures with excess NH_3.

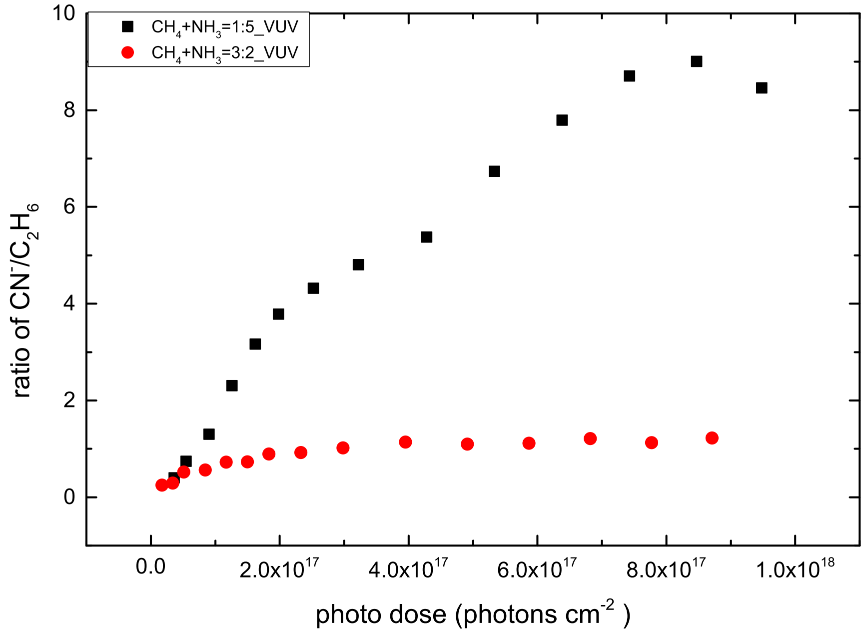

Figure 3.9: The column density of CN^- divided by C_2H_6 accumulated when different configurations of CH_4 + NH_3 ice mixtures are irradiated by VUV photons provided by MDHL.

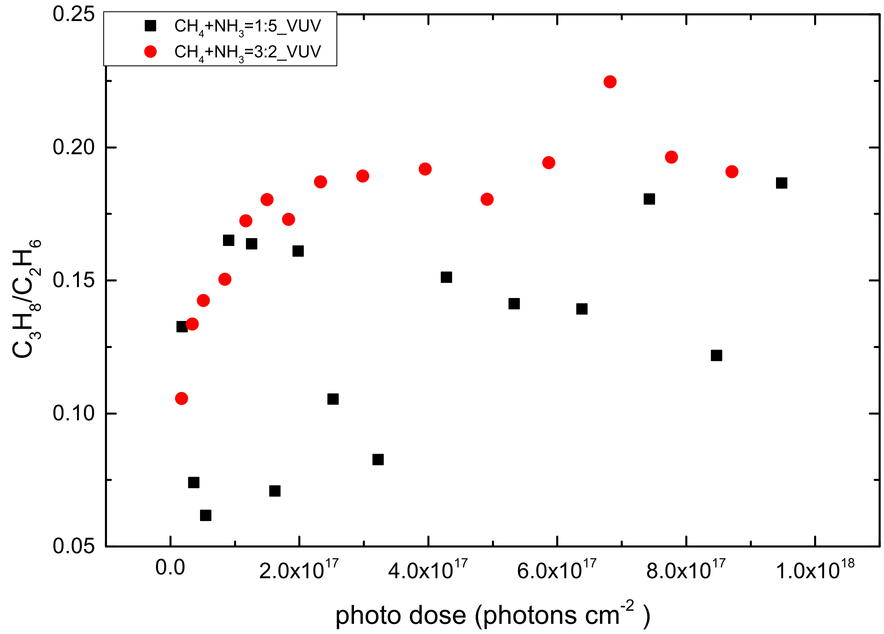

Figure 3.10: The column density of C_3H_8 divided by C_2H_6 accumulated when different configurations of CH_4 + NH_3 ice mixtures are irradiated by VUV photons provided by MDHL.

3.3.3 Propane

C_3H_8 forms based on to the C_2H_6 3.10 is the plot with column densities of C_2H_6 divided by C_3H_8. We may see that the ratio in CH_4+NH_3 =1:5 experiment is around 6 where CH_4+NH_3 =3:2 is around 3. This shows that the amount of C_3H_8 in CH_4+NH_3 =3:2 experiment is higher. It is rather difficult for C_3H_8 to form in CH_4+NH_3 = 1:5 experiments because NH_3 aggregated them. The formation of C_3H_8 in CH4+NH3 =1:5 and 3:2 experiments has given a reasonable explanation about why C_2H_6 formation is most efficient in CH_4+NH_3 =1:10 experiments.

3.4 Photon Energy Effect - EUV and VUV

According to Blanksby and Ellison [23], the dissociation energy for CH_4, becoming CH_3, CH_2 CH and C are 4.55, 4.79, 4.39 and 3.51 eV respectively at 298 K. Whereas dissociation energy for NH_3, becoming NH_2 is 4.67 eV at 298 K.

Considering our MDHL with average energy of 9.27 eV, all of the above fragments may exist either in the form of radicals or combined with other radicals to form heavier molecules in our ice mixtures. Although Increasing the photon energy does not create new fragmentation pathway, the choice of fragmentation pathways depends on photon energy.

Several gaseous state measurements also support this statement. First, Gans et al. (2011) [24] changed VUV photon wavelengths from 121.6 nm to 118.2 nm to dissociate the CH_4 molecules and ionize the fragments with the corresponding photon energy. Changing the output of the pulsed laser from 121.6 to 118.1 nm significantly changed the ratio of CH_3^+ and CH_2^+, produced from fragmentation, from 1: 1 to 1:2. This slight change of photon energy, from 10.2 eV to 10.4 eV has a significant change in the ratio between different pathways.

Second, an EUV fragmentation experiment done by Tsai et al. [25] used 30.4 nm to photo-dissociate CH_4 and tested it by timeĂŞ - of ĂŞ-flight mass spectrometer yields CH_3^+: CH_2^+: CH^+: C^+ = 1 :0.32: 0.118: 0.0237 (Tsai 1980). Consider the ratios of CH_3 to CH_2 radicals, it is around 3 to 1, which is in contrast to the experiment results of Gans et

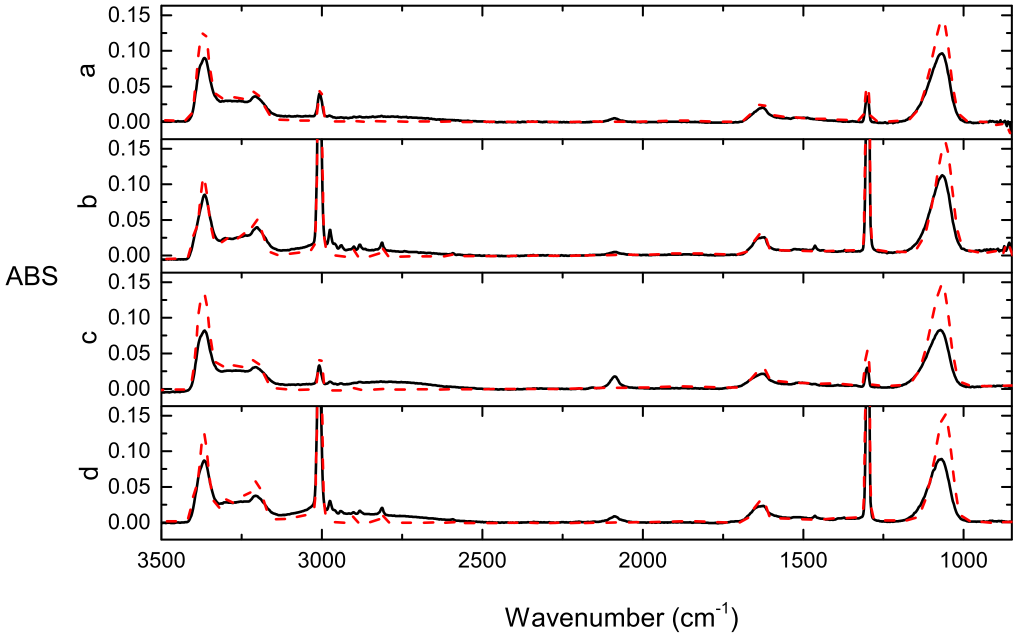

Figure 3.11: The the infra-red spectrum of $CH_4 + NH_3$ ice mixtures before irradiation (dashed) and VUV and EUV (solid) irradiated ice mixtures provided by MDHL. (a) and (b) are EUV irradiated CH_4+NH_3 = 1:5 and 3:2 ice mixtures respectively, and (c) and (d) are VUV irradiated CH_4+NH_3 = 1:5 and 3:2 ice mixtures respectively.

al. (2011)[24]. Although both of them are gaseous state experimental results, it is uncertain that if increasing photon energy can produce more CH_2 radicals.

Thirdly, a group varies ratios of $CH_4 + NH_3$ mixtures and irradiate with far UV irradiation at 134 nm [26]. However, this group only used gas chromatography to analyse the final products and their reaction is carried in gas phase in room temperature. We aware that the VUV absorption spectra of CH_4 in solid phases is different from gaseous phases [27], so the exact photo dissociation fragmentation ratios by EUV nor VUV irradiations in astronomical environments are still unknown. It is worthwhile for us to perform the experiment by EUV irradiation to see if EUV irradiation can generate any new products on the surface of Charon, or any difference in yield. Despite the photon energy of our MDHL is enough to dissociate both the CH_4 and NH_3 molecules, we further increase photon energy to He II 30.4 nm to examine the differences in photo-products.

Table 3.5 shows the identified peaks of CH_4+NH_3 ice mixtures irradiated by VUV and EUV (30.4 nm) irradiated in IR spectra (figure 3.11).

Table 3.5: The peak positions of identified substances after VUV and EUV irradiations in different configurations of ice mixtures.

Literture assignments		CH_4+NH_3 ratio (MDHL)		CH_4+NH_3 ratio (30.4 nm)		
Wavenumber (cm^{-1})	Carrier	1:5 (cm^{-1})	3:2 (cm^{-1})	1:5 (cm^{-1})	3:2 (cm^{-1})	Ref.
3375	ν_3 (NH_3)	3366	3367	3368	3368	1
3290	$2\nu_4$ (NH_3)	-	-	-	-	1
3210	ν_1 (NH_3)	3207	3205	3209	3205	1
3011	ν_3 (CH_4)	-	-	-	-	2
2972	ν_{10} (C_2H_6)	2975	2975 2977	2976		3
2960	C_3H_8	-	2960	-	2960	7
2941	$\nu_8 + \nu_1 1$ (C_2H_6)	2940	2940	-	2942	3
2904	ν_1 (CH_4)	2901	2901	2901	2901	5
2879	ν_5 (C_2H_6)	2882	2882	-	2884	3
2814	$\nu_2 + \nu_4$ (CH_4)	-	2815	-	2813	5
2083	ν (CN^-)	2088	2088	2090	2089	2
1625	ν_4 (NH_3)	1625	1631	1627	1631	1
1514	δ (NH_2)	1509	1511	1509	1511	6
1465-1440	deform CH_2 scissor	1461	1463	-	1465	3,4
1390-1370	CH_3 sym deform	1394	1372	-	1372	4
1298	ν_4 (CH_4)	1301	1299	1303	1301	2
1075	ν_2 (NH_3)	1073	1072	1070	1068	1
820	$\nu_1 2$ (C_2H_6)	-	820	-	-	3

Reference: 1. Bossa et al. 2008 [9] 2. Moore and Hudson 2003 [10] 3. Kim et al. 2010 [11] 4. Socrates 2001 [12] 5. Bennet and Kaiser 2007 [13] 6. Zheng et al. 2008 [14] 7. Hudson and Moore 2004 [15]

Considering the formation mechanisms of C_2H_6 and C_3H_8, equation (3.2 and 3.4), when MDHL VUV irradiation is replaced by He II 30.4 nm monochromatic light, the ratio of C_2H_6 to C_3H_8 in CH_4 to NH_3 = 3:2 ice mixtures irradiated by VUV irradiation is lower under EUV irradiation than that under EUV provided by NSRRC (figure 3.12). There are two possible explanations. First, different photon energies flavour different CH_4 fragmentation pathway and less C_3H_8 is produced with EUV photons. Second, the efficiency of CH_4 fragmentation is greatly reduced under EUV irradiation and the density of CH_3 radicals are much lower than that in the case of VUV irradiation provided by the MDHL. We lengthen the time of EUV irradiation on our ice mixtures until the total number of destructed CH_4 is similar to that in VUV irradiation experiments done with MDHL. The averages of ratios of C_2H_6:C_3H_8 of the last 7 irradiations before terminating irradiations are 3.53 in VUV and

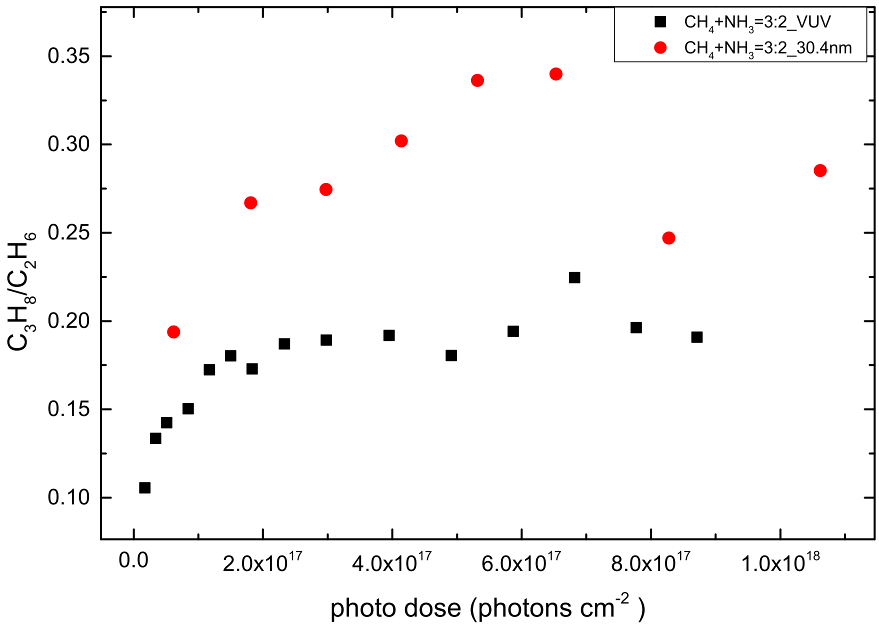

Figure 3.12: The column density of C_3H_8 divided by C_2H_6 accumulated when different configurations of CH_4 + NH_3 ice mixtures are irradiated by VUV and EUV photons

3.66 in EUV. The result supports the latter explanation. From figure 3.13, The reduction of CH_4 is 6.06± times slower in EUV experiments than VUV experiments while the reduction of NH_3 is 3.19±0.12 times lower. Therefore, the destruction cross-section of CH_4 and NH_3 ice has a 6.06±0.07 and 3.19±0.12 times lower in 30.4 nm than in 121.6 nm.

Figure 3.12 shows the column densities of C_2H_6 divided by C_3H_8 after CH_4 + NH_3 =3:2 ice mixtures are irradiated by VUV irradiation and He II monochromatic light.

From 3.12, we may observe that more C_3H_8 is produced by 30.4nm photons than by VUV photons. Recall the formation mechanism of C_3H_8 (equation 3.5), CH_2 and C_2H_4 radicals are esccential in producing C_3H_8. This increase production in C_3H_8 may be caused by the increase in CH_2 radicals during fragmentation of CH_4. This result is similar to the findings of Gans et al. (2011)[24], the ratio of CH_2 radicals increases from 0.3 to 0.48 when photon energy increases from 121.6 nm to 118.2 nm in their pulsed laser experiments.

Apart from C_2H_6 and C_3H_8, are there any difference in CN^- pro-

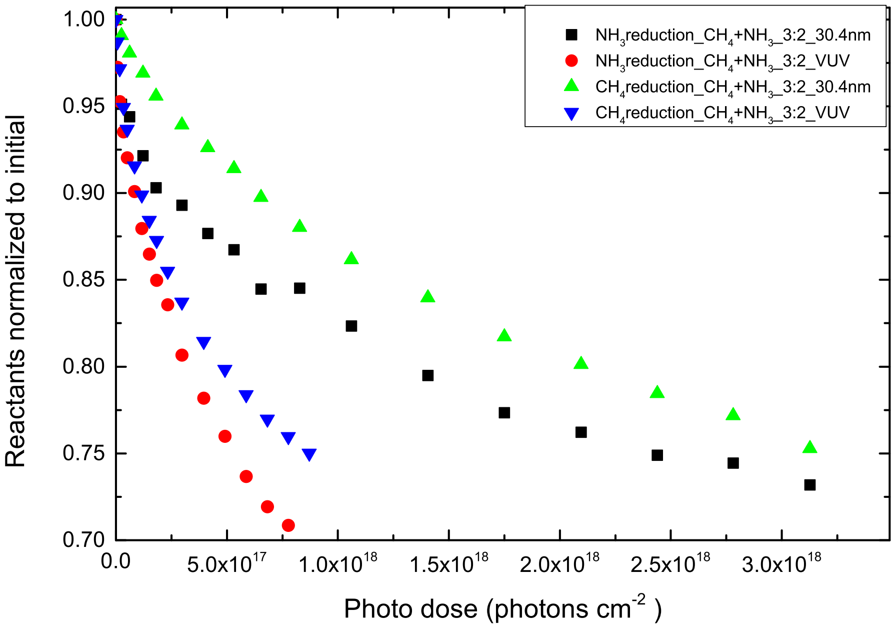

Figure 3.13: The normalized reduction of CH_4 and NH_3 in CH_4 + NH_3 ice mixtures irradiated by VUV and EUV photons

duction? Figure 3.14 shows the accumulated column densities of CN^- generated by irradiation of CH_4+NH_3 ice mixtures by MDHL and 30.4 nm monochromatic light. The fitting results are shown in Table 3.6. The rate constants forming CN^- is 3.06 to 4.13 times larger in CH_4+NH_3 = 1:5 and 3:2 irradiated by MDHL than irradiated by 30.4 nm monochromatic light respectively. From figure 3.13, the destruction cross-section of CH_4 and NH_3 are reduced by 6.06±0.07 and 3.19±0.12 times respectively. The formation rate constants of CN^- is 3.06 to 4.13 times smaller than VUV irradiations. Therefore, we may conclude that the reduction in CN^- formation rate by 30.4nm EUV irradiation is mainly due to the decreased NH_3 destruction cross-sections.

3.5 Residues

The residues we studied are the accumulated residues onto the substrate. We do not understand are there any interaction between residues and the ice mixtures. However, we may know what is the change of residues when we change the ratio of the CH_4+NH_3 from CH_4 dominating to NH_3 dominating. Figure 3.15 is a comparison of CH_4+NH_3 =

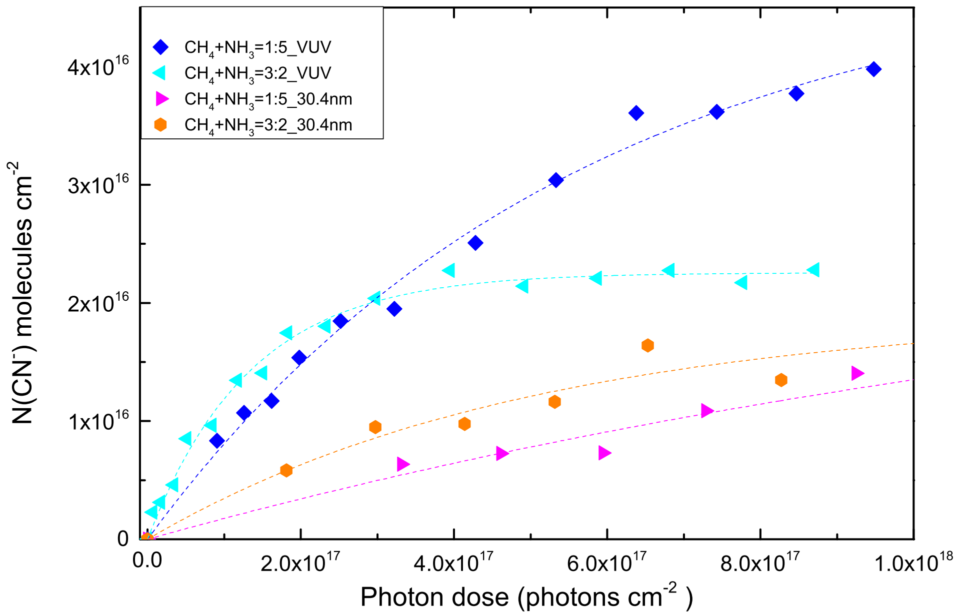

Figure 3.14: The column densities of CN^- generated by irradiation of CH_4+NH_3 ice mixtures by MDHL and 30.4 nm monochromatic light.

Table 3.6: The fitting results of CN^- by equation 2.10

Light source	Ratio of CH_4+NH_3	A (x10^{16} molecules cm^{-2})	k_1 (x10^{-18} $photon^{-1}$)	k_2 ($photon^{-1}$)
VUV	1:5	4.61 ± 0.18	1.93 ± 0.19	>1
MDHL	3:2	2.24 ± 0.03	8.21 ± 0.70	>1
EUV	1:5	2.89 ± 1.29	0.63 ± 0.37	>1
30.4nm	3:2	2.24 ± 0.03	1.92 ± 1.99	>1

Fitting result of figure 3.14 with pseudo first order equation $[CN^-]=A(1-e^{-kx})$. These fitting results of MDHL experiments are an average of at least 2 experiments with the same circumstances. In the expression, A represents the column density when x, the photon dose, becomes infinitely large and k is the rate constant.

3:2 after VUV experiments, residues accumulated after EUV exposure of CH_4 + NH_3 = 3:2 ice mixtures and the plasma experiment done by Imanaka et al. (2004)[8]. The residues in ammonia dominated ice mixtures cannot be detected after consecutive experiments. There are no differences between EUV accumulated residues and VUV accumulated residues in CH_4+NH_3 = 3:2 ice mixtues. The main differences between plasma experiments of N_2+CH_4 (9:1) done at 2300 Pa. by Imanaka et al. (2004)[8] and our experiments is the peaks located around 2090 cm^{-1}.

Why we use different initial reactants, replacing N_2 by NH_3 but we may get similar residues? The similarities during formation of atomic nitrogens when breaking N_2 bonds in nitrogen and NH bonds in ammonia give rise to this result. When photon energy is enough to break both NH bond and N_2 bond, similar experimental residues forms. Our results implies that the residues formed on Charon is similar to what we found on Titan, although their formation environments differs from gaseous phase with N_2 dominating to solid phase with NH_3.

After CH_4+NH_3 = 1:5, 1:10 and 1:20 experiments, we notice that two new bonds are formed. One at 1721 cm^{-1} and another at 1286 cm^{-1}. These two peaks are due to MCT detector self-contamination. When we stopped adding liquid nitrogen, molecules stick onto MCT detector will be free out. They sticked onto our detector and hence produced these two peaks. Hence, we may conclude that the residues produced by CH_4+NH_3 with different ratios are the same.

3.6 Conclusion

The main product of VUV and EUV irradiated CH_4+NH_3 ice mixtures are C_2H_6 and CN^-. C_3H_8 is also produced by C_2H_6 or C_2H_2. We did several investigations towards CH_4+NH_3 ice mixtures. First, by changing ratio of CH_4 and NH_3 in the ice mixture, CN^- production is more effective in NH_3 dominated ice mixtures where C_2H_6 dominates in CH_4 dominated ice mixtures. Second, by changing the photon source to EUV irradiation, the yield of C_3H_8 increases. The effective formation of C_3H_8 was not produced by C_2H_6 but by C_2H_2 and CH_4 because the ratio of C_3H_8 : C_2H_6 increases. This suggests that the CH_2 or CH fragmen-

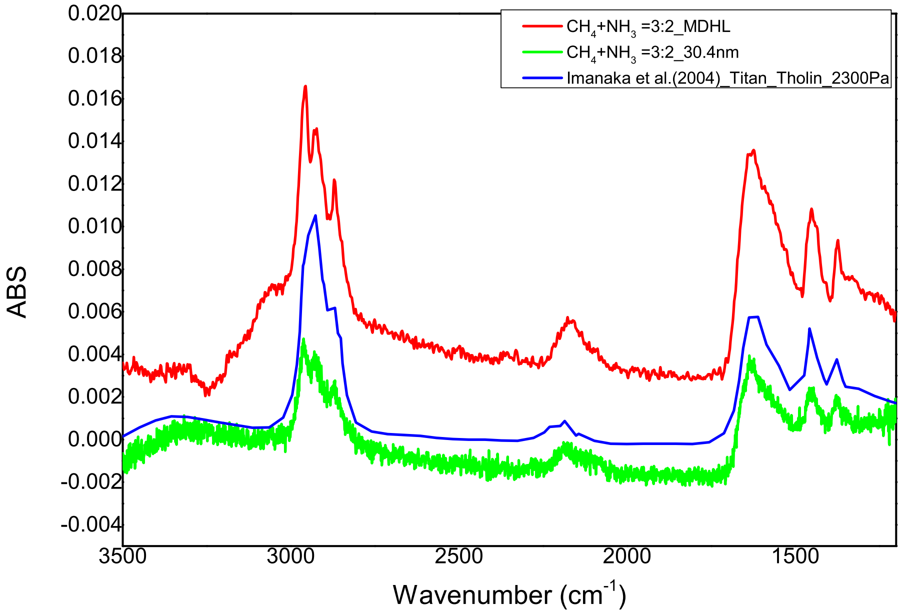

Figure 3.15: The IR spectrum of residues in after CH_4+NH_3 = 3:2 experiments and the accumulate residues after MDHL experiments and NSRRC experiments.

tation from CH_4 increases when photon energy increases. By studying the production efficiencies, the difference in photo-production yield is mainly caused by the reduction in photo-destruction cross-section in the reactants. Thirdly, by comparison with electron irradiation experiments, electron irradiation has a smaller absorption cross-sections, the percentage of yield is also smaller than VUV irradiated ice mixtures with similar ice thicknesses. Finally, we compared our residues obtained with laboratory produced Taitan tholins, the similar infra-red spectrum shows a similar functional groups in residues. Our result implies that the tholin on Charon should be similar to the tholin formed on Titan.

4. Astrophysical Implications

The main source to irradiating the dark side of Charon is Lyα reflected by interplanetary medium [1]. Other sources included energetic ions in solar wind, which mainly consist of H^+, He^+, He^{++} and O^{2+} etc. originated from solar corona or IPM. These ions also reflect solar irradiation to the dark side of Charon. Among sources focused on He II irradiation as it is 3 toĂŞ 20 times more intense than He I during a solar flare. As the intensity varies with solar activities, it is difficult to estimate the dose onto Charon. Besides, electronic flux is also present in solar wind, the flux for energetic electrons observed at the 1 A. U. position is available (http://www.swpc.noaa.gov/products/goes-electron-flux).

In this chapter, we will discuss the effects of three difference energy sources , including EUV, VUV and energetic (5 keV) electrons on production of cyanide ions and their implication on Charon. First, we compare the destructive cross-sections of these sources, and then their corresponding production yields in CN^-.

4.1 The reduction of methane and ammonia by photon sources and electrons

In electron irradiation experiments of Kim and Kaiser (2011)[22], the energy transferred to CH_4 + NH_3 ice mixtures is by linear electron transfer (LET) of 3.1 keV μm^{-1}, in the order of magnitude of the MeV cosmic rays typically transferred to the ice samples. Their dose reached 1.3 eV molecule^{-1} in 90 minutes with about 610 ML of CH_4 and 260 ML of NH_3.

The percentage of photons absorbed by CH_4 and NH_3 ice mixtures under VUV irradiation is calculated by substituting cross-sections measured by Cruz-Diaz et al. [27] and the VUV intensity spectrum of our

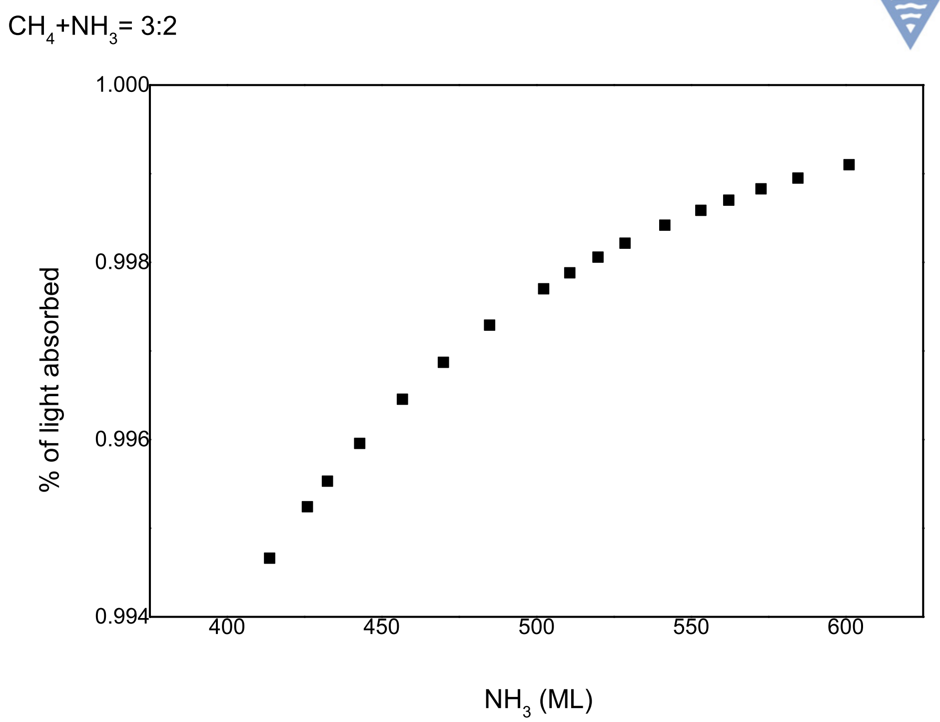

Figure 4.1: The calculated percentage of VUV irradiation absorbed by different thickness of CH_4 to NH_3 = 3:2 ice mixtures.

MDHL into Beer′s law. CH_4+NH_3 = 3:2 ice mixtures can absorb more than 99 % of light when thickness of NH_3 equals 600 ML (figure

Regarding EUV irradiations, since there are no suitable windows (used for cutting off higher order lights) to measure the absorption of ices, it is impossible to obtain absorption cross-sections right now. From figure 3.13, we obtained the distructive cross-sections of EUV to VUV photons. The CH_4 reduction by EUV photons is 6.06±0.07 times lower than VUV irradiation. From the New Horizons Mission, EUV irradiation (>12.4 eV) is $8.7 \times 10^7 eV cm^{-2} s^{-1}$ at mean heliocentric distance (39 A.U.) of Charon whereas VUV irradiation (Ly-α) is $1.9 \times 10^9 eV cm^{-2} s^{-1}$[1]. Since VUV flux is one order of magnitude more intense then EUV fluxes and the CH_4 reduction is about 6 times higher than EUV irradiation, it is the main source participants the reduction of CH_4.

4.2 Cyanide ion produced by photon sources and electrons

Considering the ice mixtures in which CH_4 is dominated, the efficiencies in CN^- formation by electrons and VUV irradiations is calculated by the final column densities divided by the column densities of the limiting reactant. A fixed amount of CN^- is obtained after irradiations. In our MDHL experiments, we have 14.8 ML of CN^- obtained in (CH_4 = 900 ML, NH_3= 600 ML) ice mixtures. Kim and Kaiser (2011) irradiated ice mixtures(CH_4 = 610 ML, NH_3= 260 ML) and obtained 13 - 16 ML of CN^- adopting the CN^- absorption coefficient (3.7×10^{-18} cm molecule^{-1}) [28], which is 4.86 times smaller than the absorption strength we adopted. We do not adopt the same absorption coefficient because the number of CN^- produced will exceed CH_4 consumption. If we adopted the same absorption coefficient, the production yield of CN^- should be multiplied by 4.86. Therefore, our yield is 72 ML of CN^-. Regarding percentage of NH_3 (limiting reactant), Kim and Kaiser has 5 - 6 % yield where we have 12 % yield if we adopted the same absorption coefficients.

The above situation is ideal to apply on the slow depositing ices or very thick ices, where photons or electrons can irradiate the surface without renewal. For fast depositing ices, this case is not suitable because only the first few layers are irradiated (figure 4.1). The depositing (hitting) rates of CH_4 onto the surface of Charon, shown in figure **??**, varies from 2 to 6×10^{11} m^{-2} s^{-1} due to the tidal locked rotation of Pluto and charon. In 1 pluto winter (130 earth years), around 110 ML of CH_4 will be deposited onto the pole positions, and 3 times more abundant than that at the pole positions facing pluto. This deposition rate is a slow depositing ice because from our experiments: figure 3.14, after 4×10^{17} VUV photons (about 1 Pluto year), maximum CN^- is formed.

As a result, under winter time, If we only consider VUV photon source, assuming ratio of CH_4 to NH_3 is 3:2, about 15 ML of CN^- will be formed during winter time, leading to similar residues as Titan.

4.3 Conclusion

Through investigating methane(CH_4) and ammonia(NH_3) ice mixtures, we better understand the followings relations: 1. The formation yield of cyanide ion (CN^-) is not proportional to the initial deposited methane when methane is dominating. However, the formation rate is proportional to its initial CH_4 to NH_3 ratios. The competition between CH_3 radicals (forming both CH_3NH_2 and C_2H_6) and NH_2 radicals (forming CH_3NH_2) results the former result. 2. When VUV is replaced by 40.8 eV 30.4nm He II EUV irradiations, the destruction cross-section of CH_4 and NH_3 are reduced by 6.06 ± 0.07 and 3.19 ± 0.12 times respectively. The lower formation rate of CN^- in EUV irradiation by 3.06 to 4.13 times is mainly due to the reduced NH_3 destruction cross-sections. 3. The photo fragmentation of CH_4 by more energetic photons are more likely to form C_3H_8 than C_2H_6, may infer there are new reaction mechanism pathways (with higher energy barrier) involved to produce C_3H_8. 4. The functional groups of residues obtained in CH_4 to NH_3 = 3:2 ice mixtures are similar to the laboratory made Titan tholins.

Bibliography

[1] W. Grundy, D. Cruikshank, G. Gladstone, C. Howett, T. Lauer, J. Spencer, M. Summers, M. Buie, A. Earle, K. Ennico *et al.*, "The formation of charon's red poles from seasonally cold-trapped volatiles," *Nature*, vol. 539, no. 7627, pp. 65–68, 2016.

[2] W. Grundy, R. Binzel, B. Buratti, J. Cook, D. Cruikshank, C. Dalle Ore, A. Earle, K. Ennico, C. Howett, A. Lunsford *et al.*, "Surface compositions across pluto and charon," *Science*, vol. 351, no. 6279, p. aad9189, 2016.

[3] W. A. Hoey, S. K. Yeoh, L. M. Trafton, D. B. Goldstein, and P. L. Varghese, "Rarefied gas dynamic simulation of transfer and escape in the pluto–charon system," *Icarus*, no. 287, pp. 87–102, 2017.

[4] J. C. Cook, S. J. Desch, T. L. Roush, C. A. Trujillo, and T. Geballe, "Near-infrared spectroscopy of charon: Possible evidence for cryovolcanism on kuiper belt objects," *The Astrophysical Journal*, vol. 663, no. 2, p. 1406, 2007.

[5] G. R. Gladstone, W. R. Pryor, and S. A. Stern, "Lyα@ pluto," *Icarus*, vol. 246, pp. 279–284, 2015.

[6] Y.-J. Chen, K.-J. Chuang, G. M. Caro, M. Nuevo, C.-C. Chu, T.-S. Yih, W.-H. Ip, and C.-Y. Wu, "Vacuum ultraviolet emission spectrum measurement of a microwave-discharge hydrogen-flow lamp in several configurations: application to photodesorption of co ice," *The Astrophysical Journal*, vol. 781, no. 1, p. 15, 2013.

[7] T.-F. Hsieh, L.-R. Huang, S.-C. Chung, T.-E. Dann, P.-C. Tseng, C. Chen, and K.-L. Tsang, "Design of a high-flux and high-resolution vuv bending-magnet beamline," *Journal of synchrotron radiation*, vol. 5, no. 3, pp. 562–564, 1998.

[8] H. Imanaka, B. N. Khare, J. E. Elsila, E. L. Bakes, C. P. McKay, D. P. Cruikshank, S. Sugita, T. Matsui, and R. N. Zare, "Laboratory experiments of titan tholin formed in cold plasma at various pressures: implications for nitrogen-containing polycyclic aromatic compounds in titan haze," *Icarus*, vol. 168, no. 2, pp. 344–366, 2004.

[9] J.-B. Bossa, P. Theulé, F. Duvernay, F. Borget, and T. Chiavassa, "Carbamic acid and carbamate formation in nh_3+co_2 ices–uv irradiation versus thermal processes," *Astronomy & Astrophysics*, vol. 492, no. 3, pp. 719–724, 2008.

[10] M. Moore and R. Hudson, "Infrared study of ion-irradiated n 2-dominated ices relevant to triton and pluto: Formation of hcn and hnc," *Icarus*, vol. 161, no. 2, pp. 486–500, 2003.

[11] Y. Kim and R. Kaiser, "Abiotic formation of carboxylic acids (rcooh) in interstellar and solar system model ices," *The Astrophysical Journal*, vol. 725, no. 1, p. 1002, 2010.

[12] G. Socrates, "Infrared and raman characteristic group frequencies, 3rd," 2001.

[13] C. J. Bennett and R. I. Kaiser, "The formation of acetic acid (ch3cooh) in interstellar ice analogs," *The Astrophysical Journal*, vol. 660, no. 2, p. 1289, 2007.

[14] W. Zheng, D. Jewitt, Y. Osamura, and R. I. Kaiser, "Formation of nitrogen and hydrogen-bearing molecules in solid ammonia and implications for solar system and interstellar ices," *The Astrophysical Journal*, vol. 674, no. 2, p. 1242, 2008.

[15] R. Hudson and M. Moore, "Reactions of nitriles in ices relevant to titan, comets, and the interstellar medium: formation of cyanate ion, ketenimines, and isonitriles," *Icarus*, vol. 172, no. 2, pp. 466–478, 2004.

[16] C. R. Richey and P. Gerakines, "Near-infrared band strengths of molecules diluted in n2 and h2o ice mixtures relevant to interstellar and planetary ices," *The Astrophysical Journal*, vol. 759, no. 1, p. 74, 2012.

[17] L. d'Hendecourt and L. Allamandola, "Time dependent chemistry in dense molecular clouds. iii-infrared band cross sections of molecules in the solid state at 10 k," *Astronomy and Astrophysics Supplement Series*, vol. 64, pp. 453–467, 1986.

[18] F. Borget, G. Danger, F. Duvernay, M. Chomat, V. Vinogradoff, P. Theulé, and T. Chiavassa, "Aminoacetonitrile characterization in astrophysical-like conditions," *Astronomy & Astrophysics*, vol. 541, p. A114, 2012.

[19] M. Moore and R. Hudson, "Infrared study of ion-irradiated water-ice mixtures with hydrocarbons relevant to comets," *Icarus*, vol. 135, no. 2, pp. 518–527, 1998.

[20] J. A. Noble, P. Theule, F. Borget, G. Danger, M. Chomat, F. Duvernay, F. Mispelaer, and T. Chiavassa, "The thermal reactivity of hcn and nh3 in interstellar ice analogues," *Monthly Notices of the Royal Astronomical Society*, vol. 428, no. 4, pp. 3262–3273, 2012.

[21] C. J. Bennett, C. S. Jamieson, Y. Osamura, and R. I. Kaiser, "Laboratory studies on the irradiation of methane in interstellar, cometary, and solar system ices," *The Astrophysical Journal*, vol. 653, no. 1, p. 792, 2006.

[22] Y. Kim and R. Kaiser, "on the formation of amines (rnh2) and the cyanide anion (cn–) in electron-irradiated ammonia-hydrocarbon interstellar model ices," *The Astrophysical Journal*, vol. 729, no. 1, p. 68, 2011.

[23] S. J. Blanksby and G. B. Ellison, "Bond dissociation energies of organic molecules," *Accounts of chemical research*, vol. 36, no. 4, pp. 255–263, 2003.

[24] B. Gans, S. Boyé-Péronne, M. Broquier, M. Delsaut, S. Douin, C. E. Fellows, P. Halvick, J.-C. Loison, R. R. Lucchese, and D. Gauyacq, "Photolysis of methane revisited at 121.6 nm and at 118.2 nm: quantum yields of the primary products, measured by mass spectrometry," *Physical Chemistry Chemical Physics*, vol. 13, no. 18, pp. 8140–8152, 2011.

[25] B. P. Tsai and J. H. Eland, "Mass spectra and doubly charged ions in photoionization at 30.4 nm and 58.4 nm," *International Journal of Mass Spectrometry and Ion Physics*, vol. 36, no. 2, pp. 143–165, 1980.

[26] A. Bossard and G. Toupance, "Far uv photolysis of ch4–nh3 mixtures and planetary studies," *Nature*, vol. 288, no. 5788, pp. 243–246, 1980.

[27] G. Cruz-Diaz, G. M. Caro, Y.-J. Chen, and T.-S. Yih, "Vacuum-uv spectroscopy of interstellar ice analogs-i. absorption cross-sections of polar-ice molecules," *Astronomy & Astrophysics*, vol. 562, p. A119, 2014.

[28] M. K. Georgieva and E. A. Velcheva, "Computational and experimental studies on the ir spectra and structure of the simplest nitriles (c1 and c2), their anions, and radicals," *International journal of quantum chemistry*, vol. 106, no. 6, pp. 1316–1322, 2006.